ERDC/CERL TR-10-26

US Army Corps
of Engineers®
Engineer Research and
Development Center

ERDC
INNOVATIVE SOLUTIONS
for a safer, better world

Prediction of Environmental Impact of High-Energy Materials with Atomistic Computer Simulations

Nandhini Sokkalingam, Jeffrey J. Potoff, Veera M. Boddu,
Stephen W. Maloney, and Joyce C. Baird

November 2010

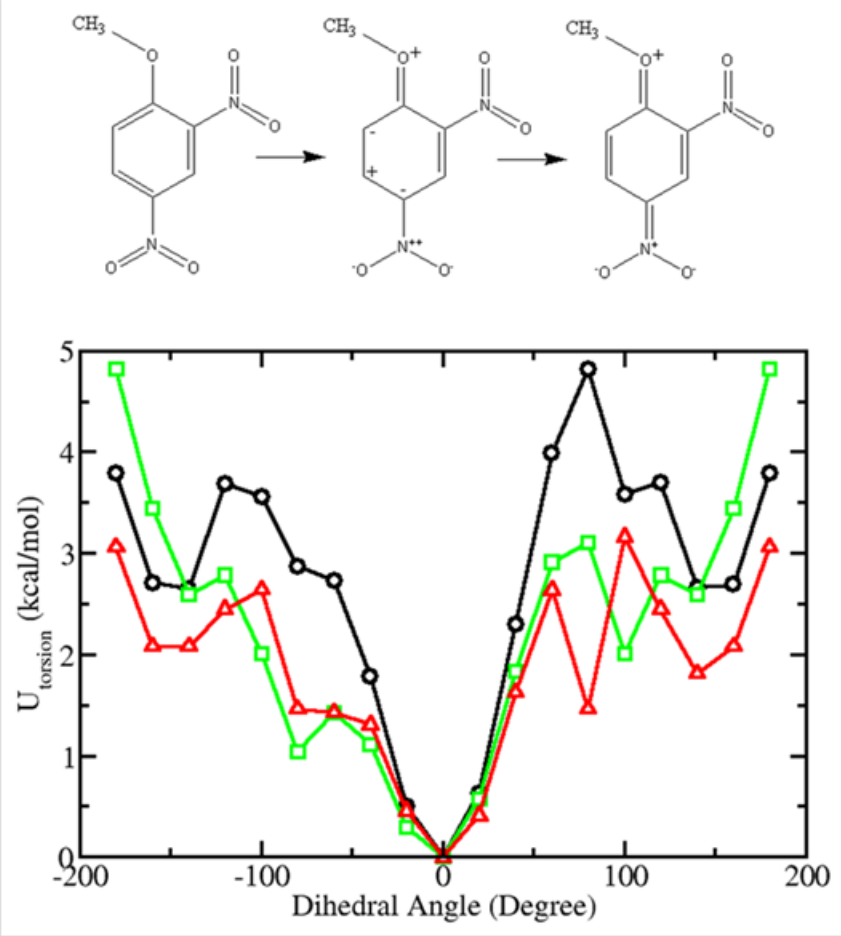

Construction Engineering
Research Laboratory

The US Army Engineer Research and Development Center (ERDC) solves the nation's toughest engineering and environmental challenges. ERDC develops innovative solutions in civil and military engineering, geospatial sciences, water resources, and environmental sciences for the Army, the Department of Defense, civilian agencies, and our nation's public good. Find out more at www.erdc.usace.army.mil.

To search for other technical reports published by ERDC, visit the ERDC online library at http://acwc.sdp.sirsi.net/client/default.

ERDC/CERL TR-10-26
November 2010

Prediction of Environmental Impact of High-Energy Materials with Atomistic Computer Simulations

Veera M. Boddu, Stephen W. Maloney, and Joyce C. Baird

Environmental Processes Branch
Construction Engineering Research Laboratory
ERDC, US Army Corp of Engineers
Champaign, IL 61826

Nandhini Sokkalingam and Jeffrey J. Potoff

Wayne State University, Department of Chemical & Materials Science Engineering
5050 Anthony Wayne Dr
Detroit, MI 48202

Final Report

Prepared for Headquarters, US Army Corps of Engineers
Washington, DC 20314-1000

Abstract

This work used atomistic molecular dynamics simulations to predict environmental impact of six energetic materials, 2,4-dinitroanisole (DNAN), N-methyl-p-nitroaniline (MNA), 3,5-dinitropyrazole (DNP), 3-nitro-1,2,4-triazol-5-one (NTO), 1-methyl-2,4,5-trinitroimidazole (MTNI) and 1,3,5-triamino-2,4,6-trinitrobenzene (TATB). Molecular models developed for these compounds were used to determine octanol-water partition coefficient (log Kow) and Henry's law constant (log H). Log Kow was predicted for DNAN and MNA to within ±0.1 log units of experiment, while log H was predicted to within ±1.0 log units. For the remaining four compounds, no experimental data exist for comparison. Predicted log Kow and log H values suggest that these compounds have the potential to cause groundwater contamination. Depending on the values of the partition coefficients, appropriate treatment methodologies can be chosen for each contaminant of interest. In addition to partition coefficients, a variety of thermophysical properties were predicted, including vapor-liquid coexistence curves, critical points, vapor pressure, heats of vaporization, crystal lattice parameters, and solid density. The crystal density and lattice parameters predicted for all energetic materials were in close agreement with experimental data. Overall, these results suggest that empirical force fields, combined with molecular dynamics simulations, provide an accurate methodology for predicting relevant descriptors of environmental fate for energetic materials.

Contents

Illustrations

Figures

Tables

Preface

This study was conducted for the Environmental Processes Branch of Engineering Research Development Center, Construction Engineering Research Laboratory (ERDC-CERL) under contract number W9132T-06-2-0027, by the Department of Chemical & Materials Science Engineering, Wayne State University, Detroit, MI. The technical monitor for this study was Dr. Reddy Damavarapu, Picatinny Arsenal, NJ (US Armament Research, Development, and Engineering Center [ARDEC]).

The work was performed by the Environmental Processes (CN-E) Branch of the Installations Division (CN), Construction Engineering Research Laboratory (CERL). The CERL Principal Investigator (PI) was Dr. Veera Mallu Boddu. Other PIs were Dr. Jeffrey J. Potoff (Associate professor in the Department of Chemical & Materials Science Engineering at Wayne State University) and Nandhini Sokkalingam (a graduate student at Wayne State University). Deborah Curtin is Chief, CN-E, and Dr. John T. Bandy is Chief, CN. The associated Technical Director is Alan B. Anderson. The Deputy Director of CERL is Dr. Kirankumar V. Topudurti, and the Director is Dr. Ilker R. Adiguzel.

CERL is an element of the US Army Engineer Research and Development Center (ERDC), US Army Corps of Engineers. The Commander and Executive Director of ERDC is COL Kevin J. Wilson, and the Director of ERDC is Dr. Jeffery P. Holland.

Unit Conversion Factors

Multiply	By	To Obtain
angstroms	0.1	nanometers
atmosphere (standard)	101.325	kilopascals
bars	100	kilopascals
degrees (angle)	0.01745329	radians
calories	4.184	joules

1 Introduction

1.1 Background

Over the past two decades, there has been considerable work in the development of insensitive munitions (IM), which exhibit low shock sensitivity and high thermal stability due to the increased safety and environmental concerns associated with the traditionally used explosives. Contamination of the environment (ground water, soil, and sediment) by explosives due to military activities such as weapon production and handling, weapons testing and training, waste discharge, and demilitarization has become a multi-billion dollar problem. Therefore, development of methodologies that can be used to predict the environmental fate of a particular compound before its deployment or even pre-synthesis is of great importance, and could lead to significant long-term cost savings.

The fate of any compound in soil, water, or the atmosphere can be determined by studying the interaction between the compound and the target medium. These interactions are described in part by partitioning the compound of interest between two different media, which is represented by various partition or distribution coefficients. Two key partition coefficients used to assess a compound's impact on air, water, and organic media are octanol-water partition coefficients and Henry's law constants (air-water partition coefficient). The Henry's law constant is the equilibrium distribution of a species between gas and liquid. For dilute aqueous solutions, Henry's law constant is the ratio of the solute's partial pressure and its aqueous concentration. Higher Henry's law constant means higher volatility and lower aqueous solubility. Octanol-water partition coefficient, which is the ratio of the concentration of a neutral chemical species in octanol and in water at equilibrium, is a measure of hydrophobicity/lipophilicity or hydrophilicity of a compound. A chemical species can be classified as hydrophobic ($\log K_{ow} > 6$) or hydrophilic ($\log K_{ow} < 0$) depending on the value of the octanol-water partition coefficient.

A wide variety of experimental techniques (Sangster 1997) exist to measure partition coefficients, but theoretical methods offer a few benefits over experiments for energetic materials. With appropriate computational methodologies, it is possible to predict the behavior of a material in the environment before it has been synthesized, allowing for a prescreening of

potential candidate molecules. Such a prescreening is expected to lead to cost savings by reducing the pool of candidate molecules for synthesis and eliminating the need for environmental remediation near manufacturing sites and test ranges. Moreover the hazardous nature and long experimental time scales associated with the development and testing of each compound makes computational methods an alternative for experiments.

Figure 1 shows the molecular structures of the six energetic materials. In this context, molecular models or "force fields" have been developed for all six compounds to predict octanol-water partition coefficient, Henry's law constant, vapor-liquid coexistence curves, critical parameters, vapor pressure, boiling point, acentric factor, heats of vaporization, lattice parameters, and crystal density. The motivation for this study comes from the work of James W. Gillett who proposed a comprehensive prebiological screen (Gillett 1983) that correlates the octanol-water partition coefficient and the Henry's law constant to predict which materials have the potential to be problematic if released to the environment.

Figure 1. Molecular structures of the energetic materials studied in this work.

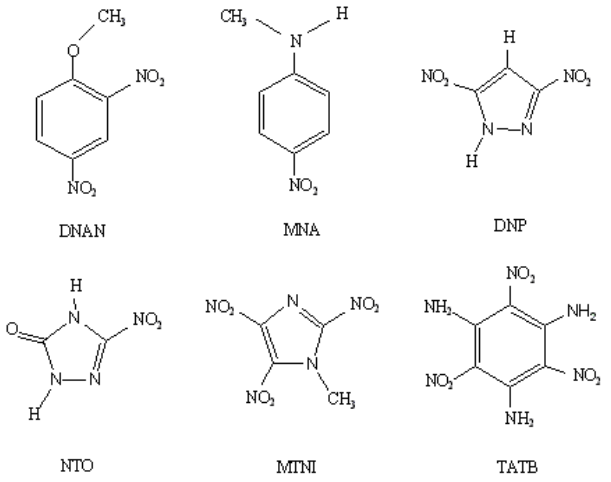

Numerous theoretical methods have been reported for the prediction of partition coefficients. Most of the computational methods are based on fragment/group or bond contribution methodology (Leo 1993; Klopman et al. 1981; Rekker et al. 1982; Suzuki et al. 1990; Rekker et al. 1979; Broto et al. 1984; Ghose et al. 1986), which use molecular descriptors (topological, topographical and quantum chemical) derived from a training set of compounds. Other methods include Quantitative Structure-Activity Relationship (QSAR) and Quantitative Structure-Property Relationship (QSPR) models (Hansch et al. 1967; Hansch et al. 1995; Bodor et al. 1989; Kantola et al. 1991; Famini et al. 1992; Moriguchi et al. 1992; Ghasemi et al. 2007), which relate the molecular structures to biological activity or other physical properties. These activities or properties are expressed as a function of the partition coefficients.

Although these methods are faster than experiments, the need for numerous empirical parameters limits their predictive capability to molecules with strong similarities to those used in the training set. Other theoretical methods offer promise as alternatives to traditional QSPR, e.g., continuum solvent methods such as COSMO (conductor screening module), SM (Solvation Model), GB/SA (Generalized Born/Surface Area models) (Still et al. 1990; Jean-Charles et al. 1991; Hawkins et al. 1998; Klamt et al. 1998; Giesen et al. 1996; Best et al. 1997) and explicit solvent methods with molecular mechanics force fields such as Monte Carlo (MC) or Molecular Dynamics (MD) coupled with free energy perturbation (FEP) (Kollman 1993; Straatsma et al. 1992). For flexible systems, the preferred method is MC or MD simulations, since these methods allow averaging over numerous molecular conformations. This work discusses the application of MD simulation to predict the pharmacokinetic properties of energetic materials.

1.2 Objectives

The objective of this research was to use molecular simulations to determine a variety of physical properties that can be used to predict the environmental fate of six IM compounds: 2,4-dinitroanisole (DNAN), N-methyl-p-nitroaniline (MNA), 3,5-dinitropyrazole (DNP), 3-nitro-1,2,4-triazol-5-one (NTO), 1-methyl-2,4,5-trinitroimidazole (MTNI) and 1,3,5-triamino-2,4,6-trinitrobenzene (TATB).

1.3 Approach

This work accomplished screening by locating coordinates for compounds in the two dimensional mobility and multimedia exposure plot (log K_{ow} vs log H), which is divided into specific regions, each characterized by a unique ecotoxicologic risk or concern like bioaccumulation, ground water pollution, and some indirect atmospheric effects like ozone depletion. Therefore knowledge of both the quantities identifies potential environmental concerns associated with each material.

1.4 Mode of technology transfer

This report will be made accessible through the World Wide Web (WWW) at URL: http://libweb.erdc.usace.army.mil

2 Conformational Analysis

It is believed that the insensitivity and thermal stability of these IM compounds are an outcome of the intramolecular and intermolecular interactions. These explosives derive most of their characteristics from the nitro and the amino functional groups. Therefore the prediction of rotational barriers offers valuable insight into the strength of these intramolecular interactions. The internal rotation mechanism around the C-N bond also yields important details of the bond rupture, which is a crucial phenomenon in the decomposition reaction of explosives. These data are also required for the development of atomistic force fields for use in MD simulations.

2.1 DNAN and MNA

The conformational behavior of DNAN and MNA was analyzed with Hartree-Fock (HF), Moller Plesset (MP2) and density functional theory (Levine 1991) using the hybrid B3LYP functional to check for other stable conformers and to obtain torsional barriers. The 6-31g+(d,p) basis set was used for all calculations.

2.1.1 Equilibrium structures

Figure 2 shows a schematic of DNAN and MNA structures. For DNAN, MP2 and B3LYP calculations predicted a co-planar structure with the methoxy group and the p-nitro group in plane with the aromatic ring, while the ortho-nitro group was tilted out of plane. The methoxy group adopted a conformation anti to the o-nitro group to avoid steric hindrance. In contrast, at the HF level of theory, the methoxy group was nearly orthogonal to the plane of the aromatic ring, with the p-nitro group in plane with the ring, and the o-nitro group out of plane with the ring.

The minimum energy conformer at the MP2 and B3LYP theories is the one with the methoxy group co-planar with the ring. At the HF theory, a perpendicular methoxy group conformation was found to be the minimum energy conformation. The O1-C1-C2 angle is 121.4 degrees at HF and decreases as the theory level increases (HF>B3LYP> MP2). The reverse (HF<B3LYP<MP2) holds true for the O1-C1-C6 angle.

Figure 2. Schematic of DNAN (left) and MNA (right).

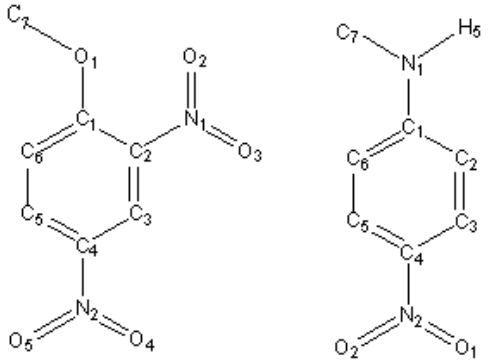

The degree of planarity of the methoxy group with the aromatic ring causes this considerable difference in the angle and leads to the tilting of the C-O bond predicted by B3LYP and MP2 theories. The repulsion between the methyl group and the hydrogen attached to C6 governs the tilting of the C-O bond. The C-C-C angles vary from 118 to 122 degrees due to the internal rearrangements that the molecule undergoes to relieve steric compression from the substituent groups. The length of the C-O bond at all level of theories and experiment (Nyburg et al. 1987) (1.33-1.35 Å) is less than the C-O bond length in anisole (1.37 Å) (Spellmeyer et al. 1990). The shortening of the C-O bond length indicates the presence of very little double bond character due to the resonance of the methoxy group with the p-nitro group. The release of electron density by the oxygen atom to the benzene ring results in an increase in electron density at the para position. A schematic of the resonance effect found in DNAN is shown in Figure 3.

Very weak hydrogen bonding is found in all levels of theories, where the oxygen from the para nitro group interacts with the adjacent hydrogen atoms, since the O-H bond (2.4 Å) is less than the sum of the van der Waals radii of oxygen and hydrogen (2.6 Å).

Figure 3. Resonance structures for DNAN.

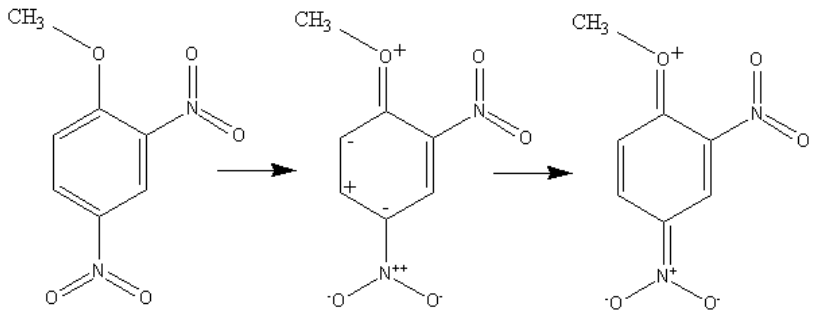

Figure 4. Resonance structures for MNA.

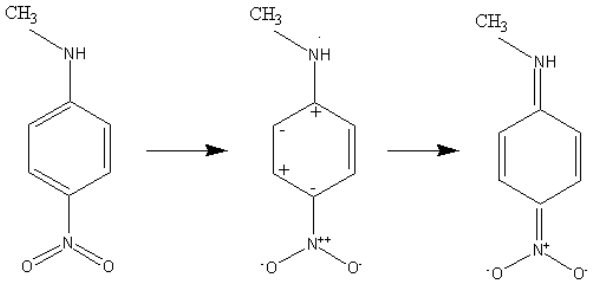

For MNA, all theories predicted a planar structure. The equilibrium parameters agree well with each other and with the experimental crystal structure (Panunto et al. 1987). The substitution of a methyl group in place of hydrogen in the amine group and conjugate effects among the strong electron-donor amine group and the phenyl ring causes the nitrogen to adopt a planar, rather than pyramidal, conformation. The equilibrium C-NH bond length was shorter than the typical equilibrium C-N single bond of 1.45 Å. The reason for shortening of the C-NH bond is due to the presence of some double bond characteristics, which are caused by the conjugate effects between the ring and the amino and nitro groups (Figure 4). Similar to DNAN, very weak intramolecular hydrogen bonding (2.4 Å) occurs in MNA for all the optimized structures.

2.1.2 Torsional barriers

Table 1 lists the predicted barriers to rotation in DNAN and MNA. Figures 5, 6, and 7, respectively, show torsional barriers for the methoxy, para- and ortho- nitro groups in DNAN. Figures 8 and 9 show torsional barriers for amino group and p-nitro group in MNA. For all the functional groups, B3LYP and HF predicted torsional barriers higher than the MP2 barriers except for the methylamine group where MP2 predicted a lower barrier than B3LYP and HF. This is due to the electron correlation effects, which are significant in these molecules.

Table 1. Rotational barriers in kcal/mol for DNAN and MNA.

	DNAN			MNA	
Theory Levels	Methoxy	O-nitro	P-nitro	Amine	P-nitro
HF	4.8	1.2	7.2	6.9	8.8
B3LYP	4.8	1.0	7.0	9.9	8.6
MP2	3.1	1.7	4.2	6.1	4.6

Figure 5. Torsional barrier methoxy group (C-O-C-C) in DNAN; B3LYP (black), MP2 (red), and HF (green).

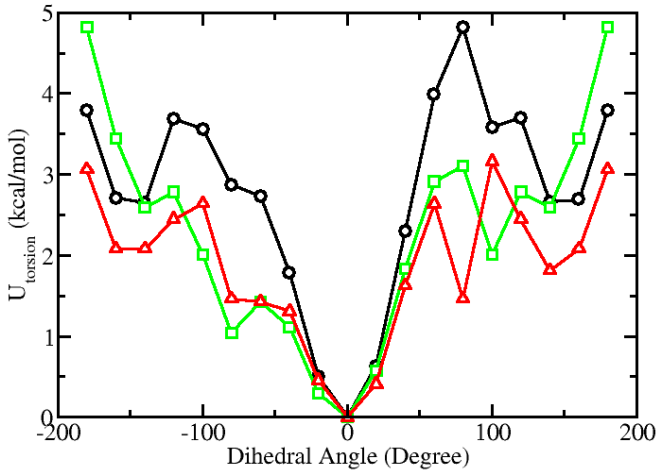

Figure 6. Torsional barrier for p-nitro group (ONCC) in DNAN; B3LYP (black), MP2 (red), and HF (green).

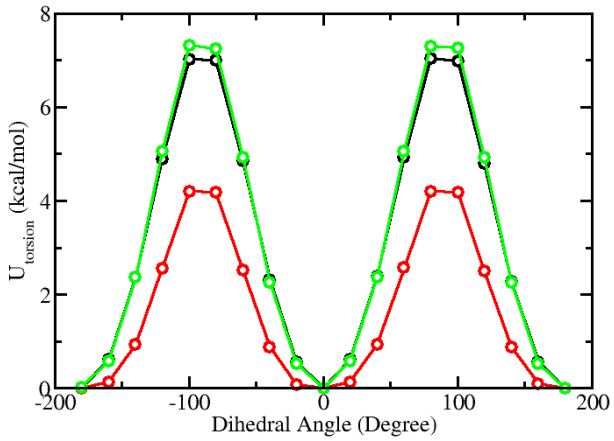

Figure 7. Torsional barrier for o-nitro group (ONCC) in DNAN; B3LYP (black), MP2 (red), and HF (green).

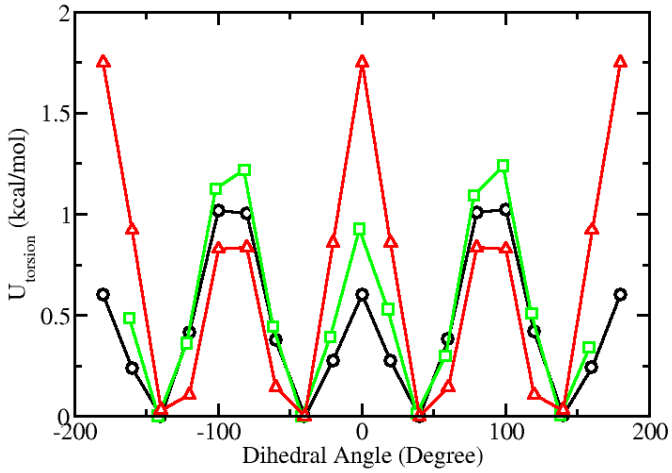

Figure 8. Torsional barrier for methylamine group (C-N-C-C) in MNA; B3LYP (black), MP2 (red), and HF (green).

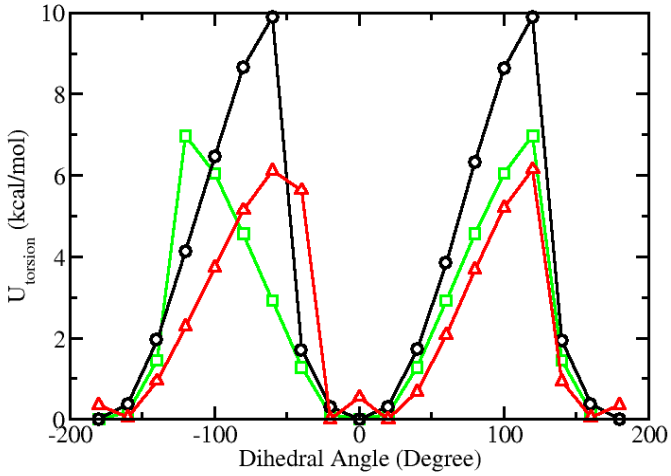

Figure 9. Torsional barrier for nitro group (O-N-C-C) in MNA; B3LYP (black), MP2(red), and HF (green).

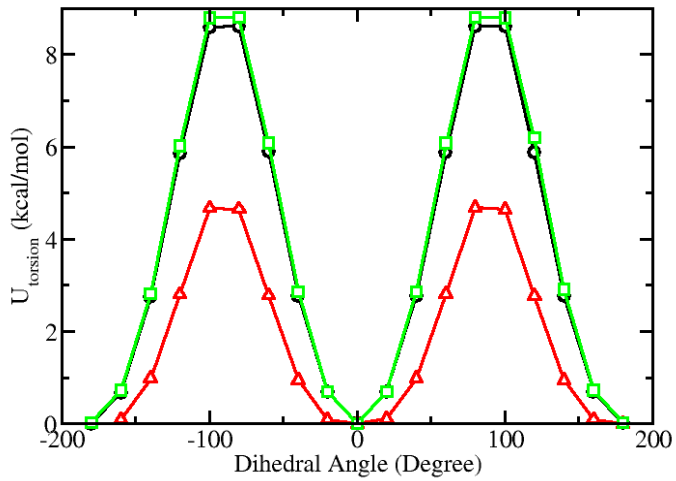

The scattered torsional curve obtained for methoxy torsion is a result of steric crowding effects between the methoxy and the bulky ortho substituent (nitro) group and conjugation between lone electron pairs on the oxygen atom and the aromatic π system. The ortho-nitro group resists the rotation of the methoxy group and eventually tilts when the methyl group approaches it to avoid overlap. This is evident from the C3-C2-N1 angle, which decreases during internal rotation of methoxy group, which indicates the drift of the ortho-nitro group, and which is manifested in the plot of rotational barriers with multiple local minima and maxima.

The barrier to torsion for amino group in MNA shows a discontinuity in energy around a dihedral angle of -50 and 150 degrees. This behavior was also observed and explained for methylamine rotation by Birkett et al.

(2002) in their work with substituted triazine rings. It is due to the ability of nitrogen in a substituted amine group to be both planar and pyramidal; when the pyramidal nature changes, there is a significant drop in energy.

As Figure 8 shows, at a dihedral angle of 0 degrees, MP2 predicts non-zero energy while B3LYP and HF theories predict 0 degrees as the lowest energy conformer. On the contrary, the equilibrium structure at the MP2 level has minimum energy for a co-planar methyl-amino group (dihedral angle of 0 degrees).

To further investigate this behavior, MP2 calculations were run with a double diffuse function (++) and larger basis set (6-311g+(d,p)), but both gave similar relative energies. Calculations performed with Quadratic Configuration Interaction Singles Doubles (QCISD) theory and 3-21g basis set predict the 0 degrees dihedral as the lowest energy conformer, in agreement with HF and B3LYP results. These results suggest that, for molecules that have resonance structures such as MNA, MP2 theory may give erroneous results for the lowest energy conformer.

2.2 DNP and NTO

2.2.1 Equilibrium structures

The optimized structures of DNP and NTO at HF, B3LYP and MP2 levels of theories are all planar with respect to the nitro groups. The molecular parameters for optimized NTO at all three levels of theories agree well with each other and the crystal structure from experiment (Bolotina et al. 2005). No experimental structure exists for DNP to make a comparison. Figure 10 shows a schematic of DNP and NTO.

2.2.2 Torsional barriers

Figures 11, 12, and 13 show the torsional barriers determined for the nitro groups in both the compounds.

Figure 10. Schematic of DNP (left) and NTO (right).

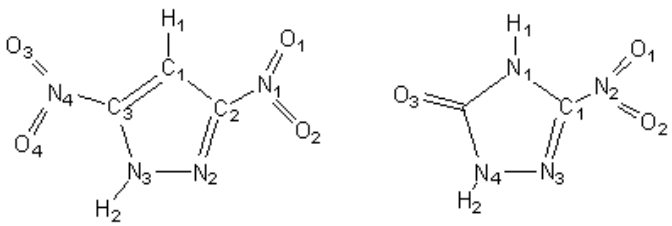

Figure 11. Torsional barriers for nitro group (O1-N1-C2-N2) in DNP; B3LYP (black), MP2 (red), and HF (green).

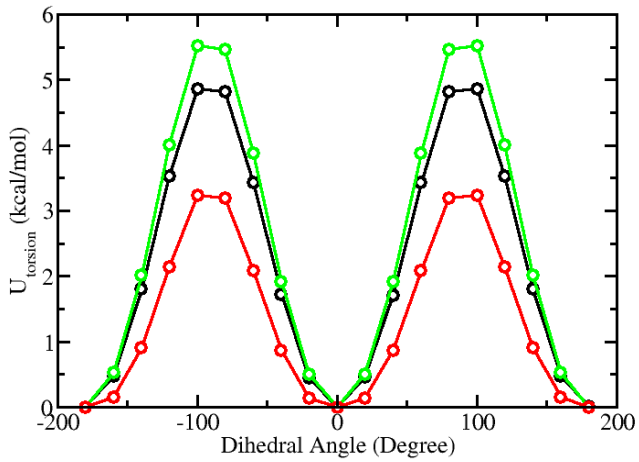

Figure 12. Torsional barriers for nitro group (O3-N4-C3-N3) in DNP; B3LYP (black), MP2 (red), and HF (green).

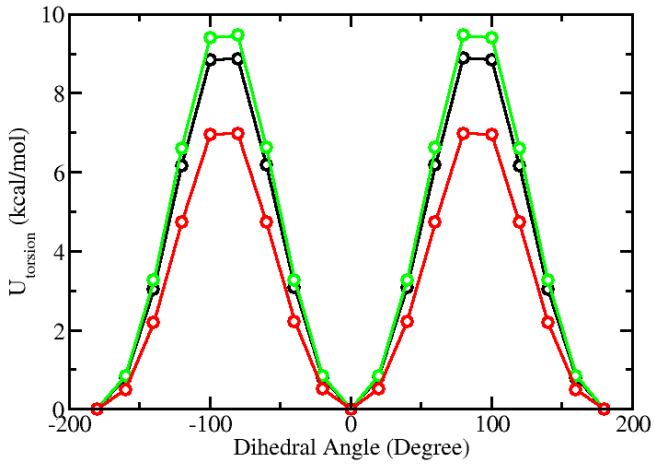

Figure 13. Torsional barriers for nitro group (O1-N2-C1-N3) in NTO; B3LYP (black), MP2 (red), and HF (green).

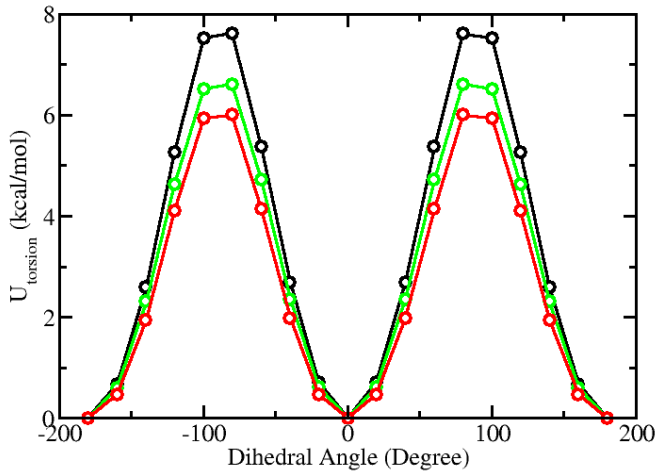

Table 2 lists the predicted barriers to rotation around the C-N bond in DNP and NTO. For DNP, the predicted barrier to rotation around the N4-C3 bond is higher than the rotation around N1-C2 bond. This is due to the location of the nitro group in each case. The nitro group at C3 is located adjacent to the amide hydrogen and involves hydrogen bonding whereas the nitro group at C2 has no amide hydrogens to bond.

Table 2. Barriers to rotation in DNP and NTO.

	DNP		NTO
Theory Levels	O1-N1-C2-N2	O3-N4-C3-N3	O1-N2-C1-N3
HF	5.5	9.4	6.6
B3LYP	4.8	8.8	7.6
MP2	3.2	6.9	6.0

3 Force Field Development

Force fields can be conveniently split into two types of interactions, bonded and non-bonded. Bonded interactions account for the conformational structure of the molecule, and include bond stretching, bond bending, and torsional rotation around the various bonds. Non-bonded interactions describe the energetics of atom-atom interactions and are usually described by an atom-atom pair interaction potential.

3.1 Non-bonded interactions

Non-bonded interactions between atoms in each molecule were represented with a standard 12-6 Lennard-Jones potential with a coulombic term for partial charges:

$$U(r_{ij}) = 4\varepsilon_{ij}\left[\left(\frac{\sigma_{ij}}{r_{ij}}\right)^{12} - \left(\frac{\sigma_{ij}}{r_{ij}}\right)^{6}\right] + \frac{q_i q_j}{4\pi\varepsilon_0 r_{ij}} \quad (1)$$

where:

r_{ij} = atom-atom separation
ε_{ij} = LJ well depth
σ_{ij} = LJ diameter
q_i = partial charge on atom i
q_j = partial charge on atom j
ε_0 = permittivity of vacuum.

Cross interaction parameters for unlike atoms were determined through Lorentz-Berthelot combining rules (Lorentz 1881; Berthelot 1898):

$$\sigma_{ij} = \frac{1}{2}(\sigma_{ii} + \sigma_{jj}) \quad (2)$$

$$\varepsilon_{ij} = \sqrt{\varepsilon_{ii}\varepsilon_{jj}} \quad (3)$$

Initial estimates of the partial charges for each molecule were determined through a CHELPG (CHarges from Electrostatic Potentials using a Grid based method) analysis by fitting to a electrostatic potential determined from *ab initio* calculations performed at the HF/6-31g+(d,p) level of theory and basis set with Gaussian 03 (Gaussian 2003). These partial charges were rescaled by a factor of 0.94 to improve the reproduction of experimentally determined octanol-water partition coefficients. Two different force fields were developed for DNAN and MNA: united-atom (UA) and

explicit hydrogen (EH). In the UA force field, all hydrogens bonded to carbon atoms are combined with carbon to form a single interaction site (a pseudo-atom) centered on the nucleus of the carbon atom. In the EH force field, all atoms are modeled explicitly, with their interaction sites centered on the respective atomic nuclei. The EH force field for DNAN and MNA was motivated by the poor performance of the UA force field in the prediction of crystal lattice parameters and solid densities. For all other compounds, only an EH force field was constructed. In this report, the united-atom force fields are referred to as DNAN-UA and MNA-UA and explicit hydrogen force fields as DNAN-EH and MNA-EH.

For the united-atom force field, Lennard-Jones parameters σ and ε for each interaction site were transferred from analogous compounds previously parameterized in the development of the TraPPE-UA force field (Martin et al. 1998; Wick et al. 2000; Stubbs et al. 2004; Wick et al. 2005**)**. In the EH version, the Lennard-Jones parameters for the nitro group were transferred from the explicit model of nitrobenzene reported in the recent work by Siepmann and co-workers (Rai et al. 2008) and the rest from the TraPPE force field (Rai et al. 2007) for five-membered rings. The aromatic ring was modeled as EH wherever necessary. The parameters for the ring were transferred from explicit model of benzene (Rai et al. 2008). Tables A1–A6 (pp 40–41) in the Appendix A to this report list the Lennard-Jones parameters and partial charges.

3.2 Bonded interactions

A harmonic term was used to represent interactions due to bond stretching:

$$U_{bond} = k_b(r - r_0)^2 \tag{4}$$

where:

k_b = force constant
r = measured bond length
r_0 = equilibrium bond length.

Bond angle bending is also represented by a harmonic potential:

$$U_{bend} = k_\theta(\theta - \theta_0)^2 \tag{5}$$

where:

k_θ = force constant
θ = measured bond length
θ_0 = equilibrium bond angle.

Barriers to rotation about various dihedral angles were controlled through a cosine series fit to *ab initio* calculations:

$$U_{tors} = \Sigma k_{\phi}[1 + cos(n\phi - f)] \quad (6)$$

where:

k_{ϕ} = force constant
ϕ = dihedral angle
n = multiplicity
f = phase angle.

4 Methodology and Simulation Details

4.1 Partition coefficients

4.1.1 Octanol-water partition coefficient

The octanol-water partition coefficient (log k_{ow}) is related to the free energy of transfer for the solute between water and water-saturated octanol phase by:

$$\Delta G = -2.303 RT \log k_{ow} \tag{7}$$

where:

R = universal gas constant
T = temperature.

Figure 14. Thermodynamic cycle used to calculate octanol-water partition coefficient.

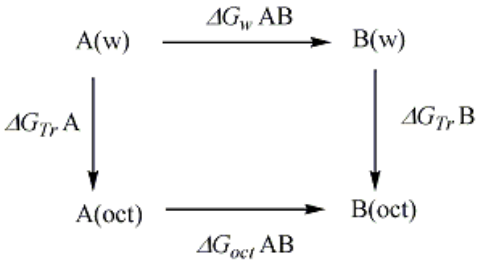

Direct calculation of free energies of transfer between water and octanol phases is possible for small solutes (Martin et al. 1997), but is extremely difficult for the larger, multi-functional molecules of interest in this work. Fortunately, because the Gibbs free energy is a state function, it is still possible to calculate the Gibbs free energy of transfer of phases through the suitable choice of path. In this work, ΔG was computed via the thermodynamic path where solute A is slowly transformed to solute B in water and water-saturated octanol (Figure 14).

This path provides a means for calculating the relative Gibbs free energy of transfer, which is defined by:

$$\Delta\Delta G_{Tr} AB = \Delta G_{Tr} B - \Delta G_{Tr} A = \Delta G_{Tr(oct)}(A \varnothing B) - \Delta G_{Tr(w)}(A \varnothing B) \tag{8}$$

where:

ΔG_{Tr} = free energy of transformation.

The relative partition coefficient is now expressed as:

$$\Delta \log k_{ow} = \frac{-\Delta\Delta G_{Tr} AB}{2.303RT} \tag{9}$$

Free energy differences are calculated by the FEP technique (Kollman 1993; Straatsma et al. 1992) combined with constant pressure-temperature MD. The FEP method involves slowly transforming solute A to solute B (either A or B is the compound of interest) by scaling the interaction potential through:

$$U(\lambda) = \lambda U_B + (1-\lambda) U_A \tag{10}$$

where:

λ =scaling parameter (value between 0 and 1).

The FEP method allows calculation of the relative Gibbs free energy of transfer $\Delta\Delta G$ from which the relative octanol-water partition coefficient (Δ log k_{ow}) is obtained. The absolute partition coefficient of target molecule B is then calculated from the reference molecule A from:

$$\log k_{ow}(B) = \Delta \log k_{ow} + \log k_{ow}(A) \tag{11}$$

4.1.2 Henry's Law constant

The Henry's law constant is the equilibrium distribution of a species between gas and liquid. For dilute aqueous solutions, it is the ratio of the solute's partial pressure and its aqueous concentration. The Henry's law constant, expressed in terms of solvation energy of a solute in water, is given by (Lin et al. 2002):

$$\log_{10} H_i = \frac{\Delta G_{i/W}^{*sol}}{RT \ln 10} + \log_{10} \frac{RT\rho_w^0}{N_A} \tag{12}$$

where:

$\Delta G_{i/W}^{*so}$ = solvation free energy of species *i* in solvent water
ρ_w^0 = number density of pure water
N_A = Avagadro's number.

The solvation free energy of solute *i* in water, or the hydration free energy, is the free energy associated with the transfer of solute from vacuum to

water. Similar to the octanol-water partition coefficient, a thermodynamic path is constructed, but the water-saturated octanol phase is replaced by the vacuum phase. Solute *i* is transformed to *j* in both water and vacuum. A relative Henry's law constant term can be derived using Equation 10 and the equation for the Henry's law constant for solute *j* given by:

$$log_{10} H_j = \frac{\Delta G^{*sol}_{j/W}}{RT\, ln 10} + log_{10} \frac{RT\rho^0_w}{N_A} \tag{13}$$

By subtracting Equation 12 from 13, an expression for relative Henry's law constant is obtained:

$$\Delta log_{10} H = \frac{\Delta G^{*sol}_{j/W} - \Delta G^{*sol}_{i/W}}{2.303RT} \tag{14}$$

The second term in both Equation 12 and 13 cancels out since the density of pure water is a constant at any specific temperature. Using the thermodynamic path, Equation 14 can be written as:

$$\Delta log_{10} H = \frac{\Delta G_{Tr(w)}(i \varnothing\ j) - \Delta G_{Tr(vac)}(i \varnothing\ j)}{2.303RT} \tag{15}$$

The absolute Henry's law constant of solute *i* is then calculated from *j*'s Henry's law constant using equation:

$$log_{10} H(j) = \Delta log_{10} H - log_{10} H(i) \tag{16}$$

The FEP technique, as implemented in NAMD simulation engine (Phillips et al. 2005), was used in the NPT ensemble for computing the partition coefficients. NAMD uses a dual topology scheme (Gao et al. 1989; Pearlman 1994), where both the initial and final states are defined concurrently. For each solute of interest, three FEP simulations were performed at 298 K and 1.013 bar; one for the water phase, one for the water-saturated 1-octanol solution, and the last for the vacuum phase.

Simulations were also run at 308 and 318 K to investigate the temperature dependence of the partition coefficients. The mole fraction of water in the octanol phase was set to the experimental value of 0.255 (Debolt et al. 1995). FEP was carried out over 20 windows where the starting six and the ending six windows were unequally spaced with very small increments to improve convergence at the end points. This methodology is known to

avoid the end-point catastrophe (Beutler et al. 1994; Pitera et al. 2002) resulting from the appearing and vanishing atoms. The windows between 0.1 to 0.9 were equally spaced at 0.1 increments. A non-bonded cutoff of 14 Å and a timestep of 1.0 fs was used. The Langevin piston Nose-Hoover method (Martyna et al. 1994; Feller et al. 1995) was used to control pressure and temperature.

The Particle Mesh Ewald (PME) technique (Essman et al. 1995) was used to calculate coulombic interactions in all MD simulations. Simulations in all phases were equilibrated for 1 ns before free energy calculations were initiated. For the calculations in vacuum, an isolated hybrid molecule was simulated without boundary conditions and a damping coefficient of 10 ps^{-1} for Langevin temperature control. The vacuum run was carried out for a total of 2.4 ns with 400 ps of equilibration and 2 ns of sampling. The in vacuo simulations require relatively longer sampling times than do solvent simulations. In water and octanol phases, FEP calculations were run for a total of 6 ns with 100 ps of equilibration and 100 ps of sampling for each window.

Three independent simulation trajectories were performed in each phase and the values averaged for the net free energy of transfer, which is used to calculate the partition coefficients. Each complete FEP simulation required 576 CPU hours, running on 2.66 GHz Intel "Clovertown" CPUs, for simulations of solutes in water, while similar calculations performed in water-saturated octanol required 960 CPU hours on similar hardware.

4.2 Vapor-liquid equilibria and vapor pressure

Gibbs-Duhem integration (Kofke 1993) was used to determine the phase coexistence curve (temperature vs density) and the vapor pressure. With the knowledge of an initial coexistence point, the Clapeyron equation is integrated to provide an estimate of coexistence points at other temperatures. The Clapeyron equation is given by:

$$\left[\frac{d\ln P}{d\beta}\right]_{\sigma} = -\frac{\Delta h}{\beta P \Delta v} \tag{17}$$

where:

P = pressure
β = 1/kT
Δh = difference in molar enthalpies of the coexisting phases
Δv = difference in molar volumes
σ indicates that the derivative is taken along the saturation line.

The method allows for the prediction of the saturation pressure at a temperature ΔT away from the known coexistence point as well. Given an estimate of the saturation pressure, NPT MD simulations are performed simultaneously for both liquid and vapor phases to determine the coexistence densities and heat of vaporization. The initial coexistence point was determined by two different methods: Grand Canonical Monte Carlo (GCMC) with histogram reweighting technique (Ferrenberg et al. 1988; Ferrenberg et al. 1989; Potoff et al. 1998) and Performance Verification Test (PVT) calculation through NPT MD simulation near the critical point. In GCMC, the insertion of molecules was enhanced through multiple first bead insertions and the application of the coupled-decoupled configurational-bias Monte Carlo method (Martin et al. 1999). The ratios of attempted moves were set to 60% particle insertions/deletions, 10% configurational-bias regrowths, 15% translations and 15% rotations.

For PVT calculations, isotherms were generated at different pressures near the critical point and densities were estimated. One isotherm, where liquid and gas coexist at a specific pressure, is chosen as the initial coexistence (P, T) condition. For Gibbs-Duhem integration, subsequent gas and liquid simulations starting from the initial coexistence point were run at low temperatures for 1 ns each with 300 ps of equilibration and 700 ps of sampling. The first coexistence simulation was carried out by integrating the Clapeyron equation with trapezoidal rule, followed by two simulations with mid-point predictor-corrector method. All subsequent simulations used the higher order Adams predictor-corrector integration scheme. A non-bonded cutoff of 14 Å without tail corrections was used for all coexistence simulations.

4.3 Solid phase calculations

4.3.1 Crystal density and lattice parameters

Force fields were validated by generating lattice parameters and crystal densities and comparing them to the experiment. These calculations require knowledge of the experimental crystal structures. For the crystal density and lattice parameter calculations, initial crystal structures were taken from the Cambridge crystallographic database (Bruno et al. 2002) and replicated in x, y, and z directions to create a supercell. NPT MD simulations were run at zero pressure and 298 K. The system was initially heated from 5 K to the target temperature of 298 K using a simulated annealing technique. The temperature and pressure control methodology is the

same as MD simulations discussed in prior sections. The system was equilibrated for 1 ns, where first 250 ps was used for equilibration, followed by 750 ps of time averaging for the cell volume. The average volume was then used to calculate the crystal density.

4.3.2 Melting point

A solid-liquid interface method based on the work of Watt et al. (2004) and Morris et al. (2002) was used to determine the melting point. A solid-liquid interfacial system was prepared as follows:

1. In the original supercell, 33% of the molecules were constrained to fixed coordinates and the rest of the molecules were allowed to move.
2. A few molecules were permanently removed from the movable region to create a solid-liquid interface.
3. The structure is then subjected to MD simulations in the NVT ensemble around 1000 K for 200 ps to create liquid regions adjacent to the fixed zone.
4. The final configuration of this run is then used for NPT simulation at temperatures close to the experimental melting point.
5. Subsequent to this, MD simulations in the NVE ensemble are used for equilibration and sampling of temperature and pressure.

This final step is repeated several times by changing the volume of the cell. The resulting temperatures and pressures are plotted and a linear regression fit is made. The temperature corresponding to the atmospheric pressure is the melting point.

5 Results and Discussion

5.1 Partition coefficients

Table 3 lists the net free energies associated with each transformation in water, water-saturated octanol, and vacuum. The superscripts denote iteration number. The values from each iteration are averaged to calculate the partition coefficients.

Figure 15 shows the computed free energies with respect to the scaling parameter λ in each phase for the nitrobenzene to MNA transformation, respectively. The free energies in the plot are averages from three iterations.

Table 3. Free energies predicted in water, water-saturated octanol and vacuum. All ΔG are reported in kcal/mol.

Transformation (w)	$\Delta G1_{Tr(w)}$	$\Delta G2_{Tr(w)}$	$\Delta G3_{Tr(w)}$	Average
Nitrobenzene – DNAN (1)	–16.68	–16.45	–16.66	–16.60 ± 0.12
Nitrobenzene – MNA (2)	–1.60	–1.70	–1.82	–1.71 ± 0.11
Pyrazole – DNP (3)	83.75	83.64	84.24	83.87 ± 0.31
Pyrazole – NTO (4)	7.16	6.56	6.42	6.71 ± 0.39
Imidazole – MTNI (5)	–84.14	–83.38	–83.97	–83.83 ± 0.39
Nitrobenzene – TATB (6)	64.26	65.54	–	64.90±0.90
Transformation (oct)	ΔG1Tr(oct)	ΔG2Tr(oct)	ΔG3Tr(oct)	Average
1	–16.15	–16.75	–16.20	–16.37 ± 0.33
2	–1.99	–1.91	–1.86	–1.92 ± 0.06
3	85.16	85.62	84.91	85.23 ± 0.36
4	9.07	9.56	9.62	9.41 ± 0.30
5	–82.80	–83.10	–84.24	–83.38 ± 0.75
6	61.19	61.63	–	61.41±0.31
Transformation (vac)	ΔG1Tr(vac)	ΔG2Tr(vac)	ΔG3Tr(vac)	Average
1	–11.46	–11.43	–11.41	–11.43 ± 0.02
2	–0.52	–0.52	–0.52	–0.52 ± 0
3	82.85	82.86	82.85	82.85 ± 0
4	13.50	13.51	13.51	13.51 ± 0
5	–81.97	–82.11	–81.74	–81.94 ± 0.18
6	51.88	51.88	–	51.88±0.0

Figure 15. Free energy change for transformation of nitrobenzene to MNA in water (black), octanol (red), and vacuum (green) at 298K and 1.013 bar.

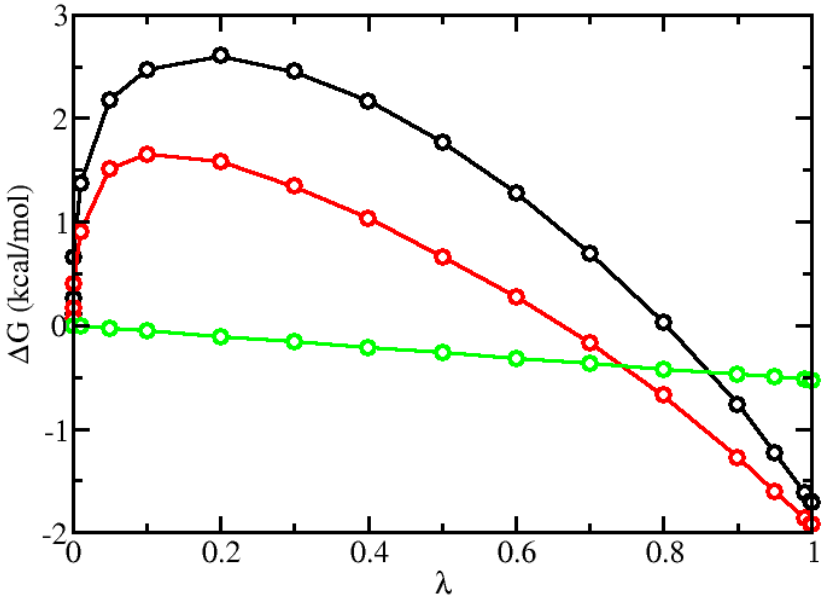

Table 4 lists the results of the convergence calculations for MNA, where *i* to *j* denote the forward perturbation and *j* to *i* the reverse perturbation. Each entry is the average of three iterations performed in each phase. The magnitude of the incremental free energies at each λ increment and the net free energy change for the forward and reverse FEP simulations agree well with each other so hysteresis is negligible and the simulations are considered converged. The change in sign is due to the difference in the direction of simulation. The free energy plots and convergence calculations are only reported for the nitrobenzene to MNA transformations, but they are representative of other transformations.

Table 4. Computed free energies (kcal/mol) in FEP simulations for MNA.

	Water		Octanol		Vacuum	
i, j	i to j	j to i	i to j	j to i	i to j	j to i
0, 0.1	2.46	–2.11	1.59	–1.51	–0.05	0.05
0.1, 0.2	0.13	–0.13	–0.04	0.05	–0.05	0.05
0.2, 0.3	0.15	–0.15	–0.25	0.21	–0.05	0.05
0.3, 0.4	0.28	–0.28	–0.33	0.32	–0.05	0.05
0.4, 0.5	0.39	–0.38	–0.36	0.38	–0.05	0.05
0.5, 0.6	0.48	–0.48	–0.38	0.44	–0.05	0.05
0.6, 0.7	0.58	–0.57	–0.44	0.49	–0.05	0.05
0.7, 0.8	0.66	–0.66	–0.50	0.52	–0.05	0.05
0.8, 0.9	–0.80	0.77	–0.57	0.53	–0.05	0.05
0.9, 1.0	–0.94	0.92	–0.65	0.68	–0.05	0.05

The absolute octanol-water partition coefficient of reference solutes nitrobenzene, pyrazole, and imidazole, and Henry's law constant of nitrobenzene and imidazole were taken from the literature (Sangster 1997; Schultz et al. 1982; Hine et al. 1975; SIDS Report 2003). Since no direct Henry's law constant has been reported in literature for pyrazole, it was calculated from experimental vapor pressure and solubility of pyrazole at 298 K by:

$$H = p / S \tag{18}$$

where:

p = vapor pressure
S = solubility.

The vapor pressure of pyrazole at 298 K is 3.638 Pa (Jimenez et al. 1987) and solubility in water at 298 K is 19.4 mol/kg of water (Wiley 1967). Tables 5 and 6, respectively, list the octanol-water partition coefficients and Henry's law constants predicted for the six energetic materials, and values predicted using COSMOtherm by Toghiani et al. (2008), EPI Suite (USEPA 2009) and experimental data (Boddu et al. 2008; Boddu et al. 2008).

Table 5. Octanol-water partition coefficient (log K_{ow}).

Molecule	Simulation	Exp	EPI	COSMO
DNAN	1.68	1.61	1.70	1.92
MNA	2.00	2.10	2.01	0.80
DNP	–0.97	—	–0.30	0.37
NTO	–1.99	—	–1.56	–1.19
MTNI	–0.40	—	0.05	1.64
TATB	–1.86	–	–1.28	4.74

Table 6. Henry's Law constants (log H).

Molecule	Simulation	EPI	Experiment
DNAN	–6.80	–3.25	–4.91
MNA	–3.88	–3.60	–6.17
DNP	–6.37	–8.62	—
NTO	–11.99	–10.77	—
MTNI	–9.24	–9.69	—
TATB	–12.56	–14.45	—

The partition coefficients from simulation are calculated by averaging the forward perturbation results. The octanol-water partition coefficients predicted by FEP simulations are within ± 0.1 log units of experiment for both DNAN and MNA. While EPI Suite values also predict octanol-water partition coefficients in good agreement with the experiment, predictions from COSMOtherm have unsigned errors of 0.12 and 1.3 log units for DNAN and MNA, respectively. Although KOWWIN (octanol-water partition coefficient prediction module in EPI) was developed with a training set of about 2500 molecules and has been tested on a dataset of 10200 compounds, it might give poor predictions for energetic materials since the training set does not include many explosive components. COSMOtherm predicts values that deviate significantly from predictions of both molecular simulations and the EPI Suite.

The Henry's law constant predicted for MNA agrees closely with the experiment while for DNAN, it is under predicted significantly. For DNAN, the source of error is unclear, since the same model was used to successfully predict log K_{ow} and the boiling point to within 10% of experiment. Although the relative partitioning between octanol and water was predicted correctly, it is possible that the model overpredicts the solubility of DNAN in water, leading to a reduced value of the Henry's law constant. Investigation of this problem is ongoing.

The EPI Suite underpredicts Henry's law constants of both DNAN and MNA. This is anticipated because HENRYWIN (Henry's law constant prediction module of EPI) relies on a much smaller calibration set of just 345 compounds (Meylan et al. 1995), therefore the predictive capabilities of the EPI Suite in this respect are more limited.

Values of Henry's law constants indicate the volatility of the compound. Compounds with Henry's law constants greater than 10^{-5} atm.m^3/mol (log H > -3.39) are considered highly volatile (Montgomery 2000). None of the energetic materials fall into this category and hence partition preferably into the aqueous phase. These findings are further illustrated by plotting the predicted partition coefficients in the multimedia-mobility plot proposed by Gillett (1983). The predicted partition coefficients are located in the heavy concern area D, which is characterized by direct effects in the water column: leaching to and flow through groundwater and plant root uptake. The compounds are not predicted to bioaccumulate or induce any atmospheric problems.

5.2 Temperature dependence of partition coefficients

The temperature dependence of the octanol-water partition coefficients and Henry's law constants were analyzed for DNAN and MNA by obtaining their values at two additional temperatures (308, 318) apart from 298 K. FEP simulations for DNAN and MNA were run at 308 and 318 K in all three phases.

Table 7 lists octanol-water partition coefficients and Henry's law constants predicted at different temperatures for DNAN and MNA, along with experimental data (Boddu et al. 2008; Boddu et al. 2008). Figure 16 shows a plot of log K_{ow} vs 1/T.

The octanol-water partition coefficients decrease with increase in temperature while Henry's law constants increase with increase in temperature. A reverse trend was observed for the MNA experimentally, where the Henry's constant decreased with increasing temperature, although the decrease is small and the statistical error in the data is unknown.

Table 7. Temperature dependence of Partition Coefficients for DNAN and MNA.

Temp (K)	DNAN				MNA			
	log K_{ow}		log H		log K_{ow}		log H	
	Sim	Exp	Sim	Exp	Sim	Exp	Sim	Exp
298	1.68	1.61	–6.80	–3.25	2.00	2.10	–3.88	–3.60
308	1.63	1.54	–6.56	–3.24	1.95	1.98	–3.83	–3.64
318	1.54	1.47	–6.47	–3.23	1.92	1.93	–3.80	–3.68

Figure 16. Octanol-water partition coefficient as a function of reciprocal temperature for DNAN (circle) and MNA (square). Filled symbols correspond to experimental values. Solid line corresponds to the linear regression fit to simulation data.

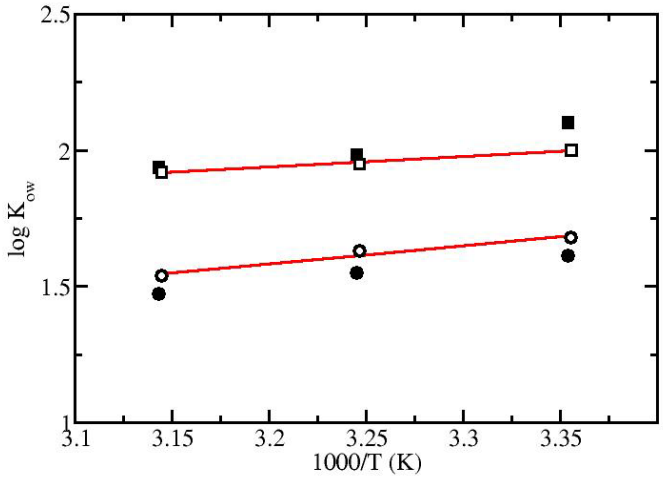

In general, experiments have shown the same trend as the simulation data, i.e., Henry's law constants increase with temperature increase (Staudinger et al. 1996). Therefore it would be advisable to perform additional experiments to identify the source of the unique behavior for the MNA Henry's constant with respect to temperature.

The data in the plots were fit to van't Hoff equation (isochore), which governs the variation of the equilibrium constant with temperature. As an equilibrium constant, log K_{ow} can be expressed as:

$$log\,K_{ow} = \frac{-\Delta H}{2.303RT} + \frac{\Delta S}{2.303R} \tag{19}$$

where:

ΔH = enthalpy of water-octanol partitioning
ΔS = entropy of water-octanol partitioning.

Enthalpy and entropy are constant over the temperature range studied. ΔH and ΔS are determined from the linear regression fit to the log K_{ow} vs 1/T plot. The Gibbs free energy of partitioning (ΔG) at a specific temperature is determined from Equation 5. Table 8 lists the enthalpy, entropy, and Gibbs free energy of partitioning for DNAN and MNA between octanol and water, along with the experimental values. For both DNAN and MNA, transfer from water to octanol is exothermic and enthalpy driven. which is evident from the negative values of ΔH. The temperature dependence of the Henry's law constant is described by the equation:

$$log\,H = \frac{-\Delta H_v}{2.303RT} + \frac{-\Delta S_v}{2.303R} \tag{20}$$

where:

ΔH_v = Enthalpy of volatilization
ΔS_v = Entropy of volatilization.

Figure 17 shows (and Table 9 lists) the enthalpy and entropy of volatilization obtained from the linear regression fit to log H vs 1/T plot.

Figure 17. Henry's law constant as a function of reciprocal temperature for DNAN (circle) and MNA (square). Filled symbols correspond to experimental values. Solid line corresponds to the linear regression fit to simulation data.

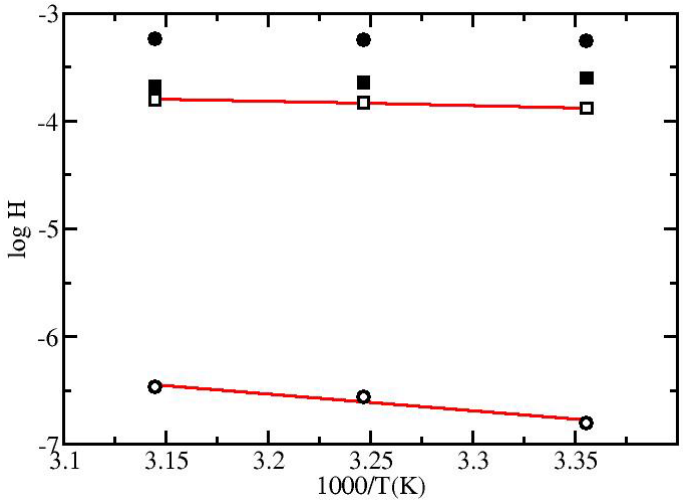

Table 8. Free energy, enthalpy, and entropy of water-octanol partitioning.

Property	DNAN		MNA	
	Sim	Exp	Sim	Exp
$\Delta G^{298\ K}$(kJ/mol)	−9.58	−9.22	−11.41	−11.95
ΔH (kJ/mol)	−12.65	−12.70	−7.27	−15.06
ΔS (J/mol/K)	−10.27	−11.68	13.83	−10.44

Table 9. Enthalpy and entropy of water-air partitioning.

Property	DNAN		MNA	
	Sim	Exp	Sim	Exp
ΔH_v (kJ/mol)	30.06	2.15	3.15	−6.62
ΔS_v (J/mol/K)	−28.86	−55.18	−21.63	−91.30

The positive enthalpy change indicates that transfer from water to gaseous state is an endothermic process. Negative entropy of transfer and a positive enthalpy term suggest that volatilization is neither enthalpy nor entropy driven (the process is not spontaneous) and the compounds have strong interactions in aqueous solution.

Vapor-Liquid Equilibria and Vapor Pressure

The force field developed for these compounds can also be used to compute other properties like critical parameters, boiling points, vapor pressure, heats of vaporization, and acentric factor. The vapor-liquid coexistence curves and critical parameters are useful in equation of state modeling of these compounds. Moreover, these properties can be used in

the development of QSPR/QSAR models, in contrast to boiling points and critical parameters derived from empirical correlations, to improve their predictive capability. Figures 18 and 19, respectively, show vapor-liquid coexistence curves and vapor pressure plots for DNAN and MNA. The phase diagrams for DNAN and MNA should be considered hypothetical, since these compounds are known to decompose at temperatures near their normal boiling points.

Figure 18. Vapor-liquid coexistence curves for DNAN (circle) and MNA (square). Line is a fit of simulation data to scaling laws. Filled symbols correspond to predicted critical points.

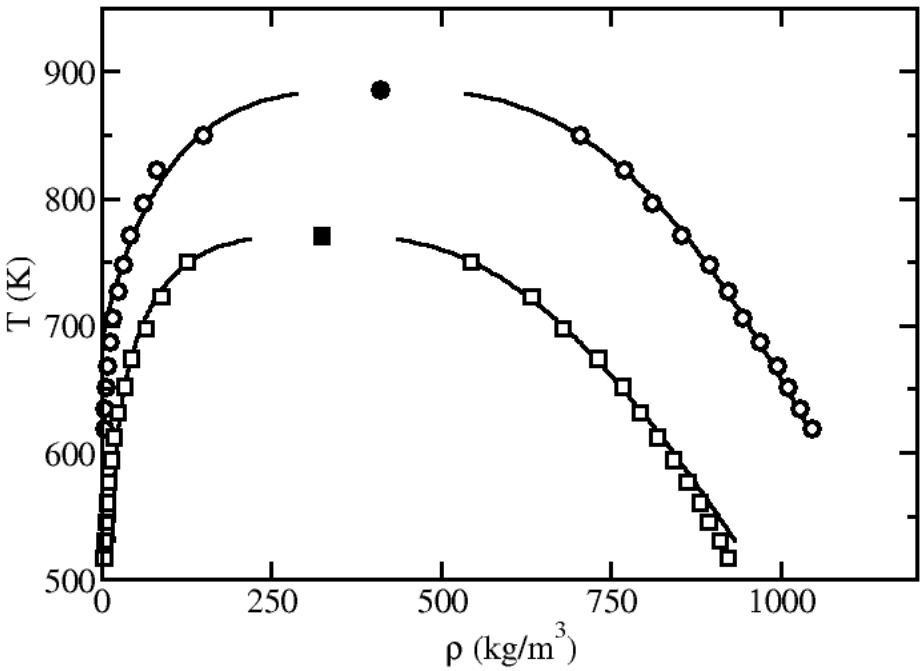

Figure 19. Clausius-Clapeyron plot for DNAN (circle) and MNA (square).

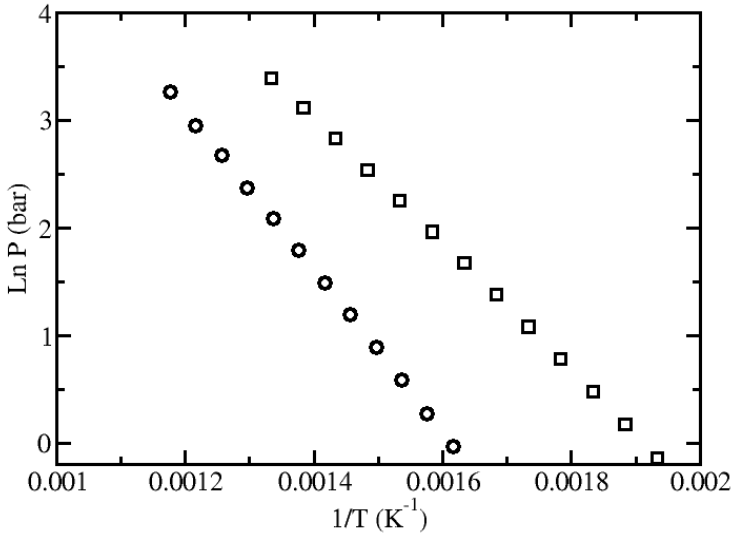

Critical temperatures and densities were computed by fitting the saturated liquid and vapor densities to the density scaling law for critical temperature (Rowlinson et al. 1982):

$$\rho_{liq} - \rho_{vap} = B(T - T_c)^{\beta} \tag{21}$$

and the law of rectilinear diameters (Rowlinson et al. 1982):

$$\frac{\rho_{liq} + \rho_{vap}}{2} = \rho_c + A(T - T_c) \tag{22}$$

where:

β = critical exponent for Ising-type fluids in 3 dimensions (0.325)
A, B = constants fit to simulation data.

Table 10 lists the critical parameters, boiling point, and acentric factor, along with values predicted through group contribution method (Stein et al. 1994) by Toghiani et al. (Toghiani et al. 2008). The experimental boiling point of DNAN at 12 mm Hg is 479 K (CRC Handbook of Chemistry & Physics, 2008-2009). The vapor pressure data from simulation were extrapolated using the Clausius-Clayperon equation to 12 mm Hg (0.016 bar). The temperature corresponding to this pressure is 461.04 K, about 3.7% lower than the experiment. The difference between the values predicted by simulation and group contribution is more pronounced for DNAN than MNA, which may be due to the proximity of the ortho-nitro group and the methoxy group in DNAN. In the force fields developed in this work, the proximity of other functional groups and synergistic effects are taken into account through the partial charge distributions, which are derived from electrostatic potential energy surfaces determined from *ab initio* calculations. For MNA, the nitro and the amine groups are far enough apart that synergy effects are expected to be negligible.

Table 10. Critical parameters, boiling point, and acentric factor for DNAN and MNA.

Molecule	T_c (K)	ρ_c (kg/m^3)	P_c (bar)	T_b (K)	ω
DNAN[a]	885.42	410.20	37.36	620.82	1.54
DNAN[b]	806	—	39.90	588	0.85
MNA[a]	770.75	324.50	37.70	522.76	1.41
MNA[b]	748	—	41.70	527	0.65

[a] This work
[b] Group Contribution

Heats of vaporization were calculated for each molecule as a function of temperature using Gibbs-Duhem integration data collected for the vapor-liquid equilibria calculations and Equation 23:

$$\Delta H_v = U_v - U_l + P(V_v - V_l) \tag{23}$$

where:

U = internal energy per mol
V = molar volume.

The subscripts v and l refer to the vapor and liquid phases, respectively. Figure 20 shows the results of these calculations.

5.3 Solid phase calculations

Tables 11 and 12 list the crystal lattice parameters and density determined for all the six compounds.

The lattice parameters and crystal density predicted for DNAN, MNA and NTO are in good agreement with the experiment. For MTNI, simulation underpredicts the c dimension and slightly over predicts the crystal density. Since experimental crystal structure is not available for DNP, solid phase calculations were not performed for it.

Melting Point

The melting point of NTO was determined using solid-liquid interface method as discussed earlier. Figure 21 shows the initial configuration used for NVE ensemble. Figure 22 shows the temperature-pressure plot.

Although pressure and temperature do not have a linear relation, the small range of temperatures (530-560 K) covered allows us to assume a linear dependence. The melting point predicted is 538.69 K, which is in excellent agreement with the experimental value of 539.35 K (Liu et al. 1995).

Figure 20. Heat of vaporization for DNAN (circle) an MNA (square) predicted from NPT MD simulations.

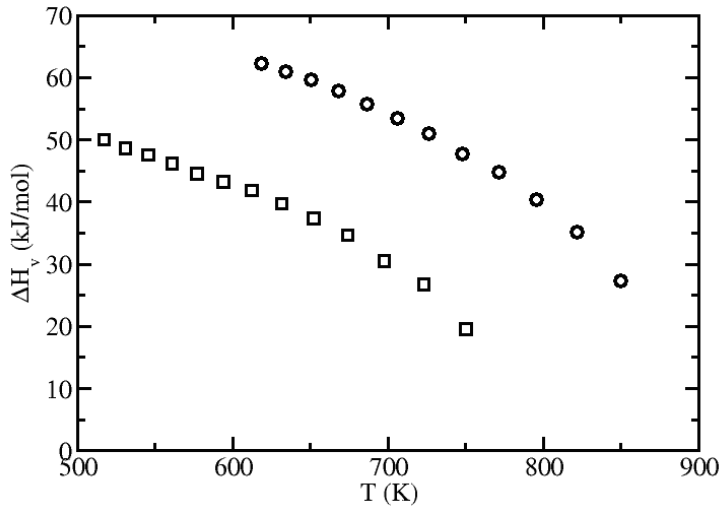

Table 11. Crystal parameters and density for DNAN, MNA, and NTO.

Parameters	DNAN (Monoclinic)		MNA (Monoclinic)		NTO (Triclinic)	
	Sim	Exp[1]	Sim	Exp[2]	Sim	Exp[3]
a (Å)	9.15	8.77	9.78	10.07	5.21	5.12
b (Å)	12.23	12.64	7.02	6.93	10.50	10.30
c (Å)	15.63	15.42	11.07	10.81	18.32	17.9
α	90	90	90	90	106.58	106.7
β	81.64	81.89	101.32	101.95	97.79	97.7
γ	90	90	90	90	90.11	90.2
ρ (g/cm³)	1.52	1.56	1.36	1.36	1.81	1.92
1 (Nyburg et al. 1987) 2 (Schaefer et al. 1988) 3 (Bolotina et al. 2005)						

Table 12. Crystal parameters and density of MTNI and TATB.

Parameters	MTNI (Orthorhombic)		TATB (Triclinic)	
	Sim	Exp[1]	Sim	Exp[2]
a (Å)	8.51	8.61	8.89	9.01
b (Å)	17.70	17.71	8.91	9.02
c (Å)	9.89	10.68	6.64	6.81
α	90	90	108.77	108.59
β	90	90	91.82	91.82
γ	90	90	119.95	119.97
ρ (g/cm³)	1.92	1.76	2.03	1.93
1 (Cho et al. 2002) 2 (Cady et al. 1965)				

Figure 21. Snapshot of initial configuration used for NVE simulations of pressure and a linear regression fit is made. The temperature corresponding to the atmospheric pressure is the melting point.

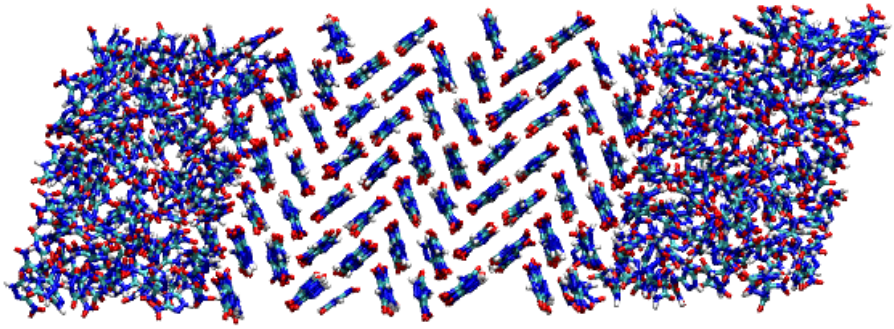

Figure 22. Temperature-pressure plot for the coexistence system.

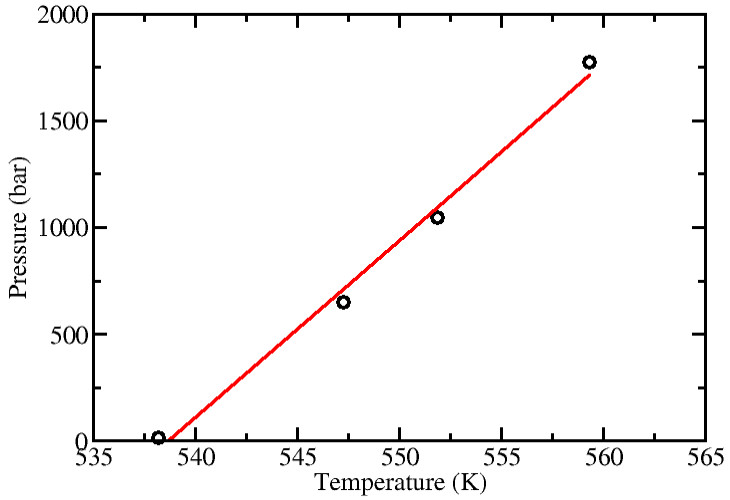

6 Conclusion

This work has demonstrated the potential of atomistic computer simulations for the prediction of partitioning and physical property prediction for energetic materials. Force fields were developed for six energetic materials (DNAN, MNA, DNP, NTO, MTNI and TATB) and the predicted thermophysical properties were found to be in close agreement (5-10% in most cases) with the scarce experimental data available. Based on the predicted octanol-water and Henry's law constants, with the exception of TATB, all compounds studied in this work are predicted to be problematic with respect to groundwater contamination.

In addition to the properties calculated in this report, the generalized, transferable force fields for energetic materials presented here may be used to investigate the interactions of energetic materials in a wide variety of complex systems, including their diffusion and transport in the environment.

Acronyms and Abbreviations

Term	Definition
ARDEC	US Armament Research, Development, and Engineering Center
CERL	Construction Engineering Research Laboratory
CHELPG	CHarges from Electrostatic Potentials using a Grid based method
COSMO	Conductor Screening Module
CPU	central processing unit
DC	District of Columbia
DNAN	2.4-dinitroanisole
DNP	3,4-Dinitropyrazole
EH	Explicit Hydrogen
EPI	Estimation Program Interface
ERDC	Engineer Research and Development Center
FEP	Free Energy Perturbation
GB/SA	Generalized Born/Surface Area
GCMC	Grand Canonical Monte Carlo
HF	Hartree-Fock
IM	Insensitive Munitions
MC	Monte Carlo
MD	Molecular Dynamics
MNA	n-Methyl-p-nitroaniline
MTNI	1-Methyl-2,4,5-trinitroimidazole
NTO	3-Nitro-1,2,4-triazol-5-one
PI	Principal Investigator
PME	Particle Mesh Ewald
PVT	Performance Verification Test
QCISD	Quadratic Configuration Interaction Singles Doubles
QSAR	Quantitative Structure-Activity Relationship
QSPR	Quantitative Structure-Property Relationship
SF	Standard Form
SIDS	Screening Information Dataset
SM	Solvation Model
TATB	1,3,5-Triamino-2,4,6-trinitrobenzene
TR	Technical Report
UA	United-Atom
URL	Universal Resource Locator
US	United States
USEPA	US Environmental Protection Agency
WWW	World Wide Web

References

Berthelot, D. C., and R. Hebd Seanc. 1898. *Acad. Sci*. 126:1703.

Best, S. A., K. M. Merz Jr., and C. H. Reynolds, 1997. GB/SA-Based continuum solvation model for octanol. *J. Phys. Chem*. 101:10479.

Beutler, T. C., A. E. Mark, R. C. van Schaik, P. R. Gerber, and W. F. van Gunsteren. 1994. Avoiding singularities and numerical instabilities in free energy calculations based on molecular simulations. *Chem. Phys. Lett*. 222:529.

Birkett, H. E., J. C. Cherryman, A. M. Chippendale, P. Hazendonk, and R. K. Harris. 2002. Molecular modelling studies of side-chain rotation in substituted triazine rings. *J. Mol. Struct*. 602:59.

Boddu, V., K. Abburi, S. Maloney, and D. Reddy. 2008. Thermophysical properties of an insensitive munitions compound, 2,4-dinitroanisole. *J. Chem. Eng. Dat*. 53:1120.

Boddu, V., K. Abburi, S. Maloney, and D. Reddy. 2008. Physicochemical properties of an insensitive munitions compound, N-methyl-4-nitroaniline (MNA). *J. Hazard*. Mat. 155:288.

Bodor, N., Z. Gabanyi, and C. J. Wong. 1989. A new method for the estimation of partition coefficient. *J. Am. Chem. Soc*. 111:3783.

Bolotina, N. B., K. Kirschbaum, and A. A. Pinkerton. 2005. Energetic materials: Alpha-NTO crystallizes as a four component triclinic twin. *Acta. Cryst. Sect B. Sruct. Sci*. 61:577.

Broto, P., G. Moreau and C. Vandycke. 1984. Molecular structures: Perception, autocorrelation descriptor and SAR studies. Perception of molecules: topological structure and 3-dimensional structure. *J. Med. Chem. -Chim. Ther*. 19:61.

Bruno, I. J., J. C. Cole, P. R. Edgington, M. K. Kessler, C. F. Macrae, P. Mccabe, J. Pearson, and R. Taylor. 2002. New software for searching the Cambridge Structural Database and visualizing crystal structures. *Acta Cryst*. B58:389.

Cady, H. H., and A. C. Larson. 1965. The crystal structure of 1,3,5-triamino-2,4,6-trinitrobenzene. *Acta Cryst*. 18:485.

Cho, J. R., K. J. Kim, S. G. Cho, and J. K. Kim. 2002. Synthesis and characterization of 1-methyl-2,4,5-trinitroimidazole (MTNI). *J. Heterocycl. Chem*. 39:141.

CRC Handbook of Chemistry and Physics. 2008-2009. Boca Raton, FL: CRC Press/Taylor and Francis.

Debolt, S. E., and P. A. Kollman. 1995. Investigation of structure, dynamics and solvation in 1-octanol and its water-saturated solution: Molecular dynamics and free-energy perturbation studies. *J. Am. Chem. Soc*. 117:5316.

Essman, U., L. Perera, and M. L. Berkowitz. 1995. A smooth particle mesh Ewald method. *J. Chem. Phys.* 103:8577.

Famini, G. R., C. A. Penski, and L. Y. Wilson. 1992. Using theoretical descriptors in quantitative structure activity relationships: Some physicochemical properties. *J. Phys. Org. Chem.* 5:395.

Ferrenberg, A. M., and R. H. Swendsen. 1988. New Monte Carlo technique for studying phase transitions. *Phys. Rev. Lett.* 61:2635.

Ferrenberg, A. M., and R. H. Swendsen. 1989. Optimized Monte Carlo data analysis. *Phys. Rev. Lett.* 63:1195.

Gaussian 03, Revision A.1. 2003. Gaussian, Inc., Pittsburgh PA.

Gao, J., K. Kuczera, B. Tidor, and M. Karplus. 1989. Hidden thermodynamics of mutant proteins: A molecular dynamics analysis. *Science* 244:1069.

Ghasemi, J., and S. Saaidpour. 2007. Quantitative structure–property relationship study of n-octanol–water partition coefficients of some of diverse drugs using multiple linear regression. *Anal. Chim. Acta* 604:99.

Ghose, A. K., and G. M. Crippen. 1986. Atomic physicochemical parameters for three-dimensional structure-directed quantitative structure-activity relationships. 1. Partition coefficients as a measure of hydrophobicity. *J. Comput. Chem.* 7:565.

Giesen, D. J., M. Z. Gu, C. J. Cramer, and D. G. Truhlar. 1996. A universal organic solvation model. *J. Org. Chem.* 61:8720.

Gillett, J. W. 1983. A comprehensive prebiological screen for ecotoxicologic effects. *Environmental Toxicology and Chemistry* 2:463.

Hansch, C., and S. M. Anderson. 1967. The effect of intramolecular bydrophobic bonding on partition coefficients. *J. Org. Chem.* 32:3583.

Hansch, C., and A. Leo. 1995. *Exploring QSAR Fundamentals and Applications in Chemistry and Biology*. Washington DC: ACS.

Hawkins, G. D., D. A. Liotard, C. J. Cramer, and D. G. Truhlar. 1998. OMNISOL: Fast prediction of free energies of solvation and partition coefficients. *J. Org. Chem.* 63:4305.

Hine, J., and P. K. Mookerjee. 1975. The intrinsic hydrophilic character of organic compounds. Correlations in terms of structural contributions. *J. Org. Chem.* 40:292.

Jean-Charles, A., A. Nicholls, K. Sharp, B. Honig, A. Tempczyck, T. F. Hendrickson, and W. C. Still. 1991. Electrostatic contributions to solvation energies: Comparison of free energy perturbation and continuum calculations. *J. Am. Chem. Soc.* 113:1454.

Jimenez, P., M. V. Roux, C. Turrion and F. Gomis. 1987, Thermochemical properties of N-heterocyclic compounds. I: Enthalpies of combustion, vapour pressures and enthalpies of formation of pyrazole, imidazole, indazole, and benzimidazole. *J. Chem. Therm*. 19:985.

Kantola, A., H. O. Villar, and G. H. Loew. 1991. Atom based parametrization for a conformationally dependent hydrophobic index. *J. Comput. Chem*. 12:681.

Klamt, A., V. Jonas, T. Buerger, and J. C. W. Lohrenz. 1998. Refinement and parametrization of COSMO-RS. *J. Phys. Chem*. 102:5074.

Kofke, D. A. 1993. Direct evaluation of phase coexistence by molecular simulation via integration along the saturation line. *J. Chem. Phys*. 98:4149.

Kollman, P. 1993. Free energy calculations: Applications to chemical and biochemical phenomena. *Chem. Rev*. 93:2395

Leo, A. 1993. Calculating log Poct from structures. *Chem. Rev*. 93:1281.

Levine, I. N. 1991. *Quantum Chemistry*. New Jersey: Prentice Hall.

Lin, S-T., and S. I. Sandler. 2002. Henry's law constant of organic compounds in water from a group contribution model with multipole corrections. *Chemical Engineering Science* 57:2727.

Liu, Z. R., Y. H. Shao, C. M. Yin and Y. H. Kong. 1995. Measurement of the eutectic composition and temperature of energetic materials. Part 1. The phase diagram of binary systems. Thermo him. *Acta* 250:65.

Lorentz, H. A. 1881. *Ann. Phys*. 12:127.

Martin, M. G., and Siepmann, J. I. 1997. Predicting multicomponent phase equilibria and free energies of transfer for alkanes by molecular simulation. *J. Am. Chem. Soc*. 119:8921.

Martin, M. G., and J. I. Siepmann. 1998. Transferable Potentials for Phase Equilibria. 1. United-Atom Description of n-Alkanes. *J. Phys. Chem*. B 102:2569.

Martin, M. G., and J. I. Siepmann. 1999. Novel configurational-bias Monte Carlo method for branched molecules. Transferable potentials for phase equilibria. 2. United-atom description of branched alkanes. *J. Phys. Chem*. 103:4508.

Martyna, G. J., D. J. Tobias, and M. L. Klein. 1994. Constant pressure molecular dynamics algorithms. *J. Chem. Phys*. 101:4177.

Meylan, W. M., and P. H. Howard. 1995. Atom/fragment contribution method for estimating octanol-water partition coefficients. *J. Pharm. Sci*. 84:83.

Montogomery, J. H. 2000. *Groundwater chemicals desk reference*. 3d ed. CRC Press.

Moriguchi, I., S. Hirono, Q. Liu, I. Nakagome, Y. Matsushita. 1992. Simple method of calculating octanol/water partition coefficient. *Chem. Pharm. Bull*. 40:127.

Morris, J. R., and X. Song. 2002. The melting lines of model systems calculated from coexistence simulations. *J. Chem. Phys*. 116:9352.

Nyburg, S. C., C. H. Faerman, and L. Prasad. 1987. Structures of 2,4-dinitroanisole and 2,6-dinitroanisole. *Acta Cryst*. 43:686.

Panunto, T. W., Z. Urbanczyk-Lipkowska, R. Johnson and M. C. Etter. 1987. Hydrogen-bond formation in nitroanilines: The first step in designing accentric materials. *J. Am. Chem. Soc*. 109:7786.

Pearlman, D. A. 1994. A comparison of alternative approaches to free energy calculations. *J. Phys. Chem*. 98:1487.

Phillips, J. C., R. Braun, W. Wang, J. Gumbart, E. Tajkhorshid, E. Villa, C. Chipot, R. D. Skeel, L. Kale, and K. Schulten. 2005. Scalable molecular dynamics with NAMD. *J. Comp. Chem*. 26:1781.

Pitera, J. W., and W. F. van Gunsteren. 2002. A comparison of non-bonded scaling approaches for free energy calculations. *Mol. Sim*. 28:45.

Potoff, J. J., and A. Z. Panagiotopoulos. 1998. Critical point and phase behavior of the pure fluid and a Lennard-Jones mixture. *J. Chem. Phys*. 109:10914.

Rai, N., J. I. Siepmann. 2007. Transferable potentials for phase equilibria. 9. Explicit hydrogen description of benzene and five-membered and six-membered heterocyclic aromatic compounds. *J. Phys. Chem*. 111:10790.

Rai, N., D. Bhatt, J. I. Siepmann, and L. E. Fried. 2008. Monte Carlo simulations of 1,3,5-triamino-2,4,6-trinitrobenzene (TATB): Pressure and temperature effects for the solid phase and vapor-liquid phase equilibria. *J. Chem. Phys*. 129:194510.

Rekker, R. F., and H. M. De Kort. 1979. The hydrophobic fragmental constant; an extension to a 1000 data point set. *Eur. J. Med. Chem. Chim. Ther*. 14:479.

Rekker, R. F., and R. Manhold. 1982. *Calculation of Drug Lipophilicity*. New York: VCH.

Rowlinson, J. S., and B. Widom. 1982. *Molecular Theory of Capillarity*. Oxford: Clarendon Press.

Rowlinson, J. S., and F. L. Swinton. 1982. *Liquids and Liquid Mixtures*. 3d ed., Butterworth.

Sangster, J. 1997. *Octanol-Water Partition Coefficients: Fundamentals and Physical Chemistry*. Wiley Series in Solution Chemistry. Vol. 2. New York: John Wiley & Sons, Ltd.

Schultz, T. W., and M. Cajina-Quezada. 1982. Structure-toxicity relationships of selected nitrogenous heterocyclic compounds II. Dinitrogen molecules. *Arch. Environ. Contam. Toxicol*. 11:353.

SIDS Initial Assessment Report. 2003. Italy: SIAM 17.

Spellmeyer, D. C., P. D. J. Grootenhius, M. D. Miller, L. F. Kuyper and P. A. Kollman. 1990. Theoretical investigations of the rotational barrier in anisole: *ab initio* and molecular dynamics study. *J. Phys. Chem*. 94:4483.

Stein, S. E., and R. L. Brown. Estimation of normal boiling points from group contributions. 1994. J. Chem. *Inf. Comput. Sci*. 34:581.

Still, W. C., A. Tempczyk., R. C. Hawley., and T. F. Hendrickson. 1990. Generalized Born equation. *J. Am. Chem. Soc*. 112:6127.

Straatsma, T. P., and J. A. McCammon. 1992. Computational Alchemy. *Ann. Rev. Phys. Chem*. 43:407.

Stubbs, J. M., J. J. Potoff, and J. I. Siepmann. 2004. Transferable Potentials for Phase Equilibria. 6. United-Atom Description for Ethers, Glycols, Ketones, and Aldehydes. *J. Phys. Chem*. B 108:17596.

Suzuki, T., and Y. J. Kudo. 1990. Automatic log P estimation based on combined additive modeling methods. *J. Comput. Aided Mol. Des*. 4:155.

Toghiani, R. K., H. Toghiani, S. W. Maloney, and V. M. Boddu. 2008. Prediction of physicochemical properties of energetic materials. *Fluid Phase Equilibria* 264:86.

Watt, S. W., J. A. Chisholm, W. Jones, and S. Motherwell. 2004. A molecular dynamics simulation of the melting points and glass transition temperatures of myo- and neo-inositol. *J. Chem. Phys*. 121:9565.

Wick, C. D., M. G. Martin, and J. I. Siepmann. 2000. Transferable potentials for phase equilibria. 4. United-atom description of linear and branched alkenes and alkylbenzenes. *J. Phys. Chem*. 104:8008.

Wick, C. D., J. M. Stubbs, N. Rai, and J. I. Siepmann. 2005. Transferable potentials for phase equilibria. 7. Primary, secondary, and tertiary amines, nitroalkanes and nitrobenzene, nitriles, amides, pyridine, and pyrimidine. *J. Phys. Chem*. 109:18974.

Wiley, R. H. 1967. *Pyrazoles, Pyrazolines, Pyrazolidines, Indazoles and Condensed Rings*. New York: Interscience Publishers.

Appendix A: Lennard-Jones Parameters and Partial Charges

Table A1. Lennard-Jones parameters for DNAN (UA).

Site	Molecule	σ (Å)	ε (K)	q(e)
C_α	Ether	4.50	15	0.150
C_α	Nitro	4.50	15	0.112
CH	Benzene	3.74	48	0.00
CH_3	Ether	3.75	98	0.252
O	Ether	2.80	55	–0.402
N	Nitro	3.31	40	0.768
O	Nitro	2.90	80	–0.440

Table A2. Lennard-Jones parameters for MNA (UA).

Site	Molecule	σ (Å)	ε (K)	q(e)
C_α	Nitro	4.50	15	0.131
C_α	Amine	4.50	15	0.187
CH	Benzene	3.74	48	0.00
CH_3	Amine	3.75	98	0.234
N	Nitro	3.31	40	0.711
N	Amine	3.52	58	–0.730
O	Nitro	2.9	80	–0.449
H	Amine	0	0	0.365

Table A3. Lennard-Jones parameters for DNAN (EH).

Site	Molecule	σ (Å)	ε (K)	q(e)
C_α	Ether	3.60	30.7	0.150
C_α	Nitro	3.60	30.7	0.090, 0.142
C-(H)	Ring	3.60	30.7	–0.165, –0.165, –0.189
H-C	Ring	2.36	25.45	0.165, 0.165, 0.189
C	Methyl	3.6	47	0.132
H	Methyl	2.5	10	0.041
O	Ether	2.80	55	–0.407
N	Nitro	2.90	30	0.774, 0.723
O	Nitro	2.70	42	–0.432`

Table A4. Lennard-Jones parameters for MNA (EH).

Site	Molecule	σ (Å)	ε (K)	q(e)
C_α	Nitro	3.60	30.7	0.194
C_α	Amine	3.60	30.7	0.133
C-(H)	Ring	3.60	30.7	–0.151, –0.135, –0.135, –0.151
H-(C)	Ring	2.36	25.45	0.151, 0.135, 0.135, 0.151
C	Methyl	3.6	47	0.197
H	Methyl	2.5	10	0.012
N	Nitro	2.90	30	0.715
N	Amine	3.26	160	–0.736
O	Nitro	2.70	42	–0.454
H	Amine	0.50	12	0.369

Table A5. Lennard-Jones parameters for DNP.

Site	Molecule	σ (Å)	ε (K)	q(e)
N	Nitro	2.90	30	0.702
O	Nitro	2.70	42	–0.414
N	Sp2	3.20	57	–0.396
C	Nitro	3.60	30.7	0.354
N	Amide	3.40	141	–0.023
H	Amide	0.50	12	0.321
C	Sp2	3.60	30.7	–0.309
H	Attached to ring carbon	2.36	25.45	0.206

Table A6. Lennard-Jones parameters for NTO.

Site	Molecule	σ (Å)	ε (K)	q(e)
O	Nitro	2.70	42	–0.416
N	Nitro	2.90	30	0.722
C	Sp2	3.60	30.7	0.408
N	Sp2	3.20	57	–0.387
N	Amide1(attached to sp2 nitrogen)	3.40	141	–0.187
H	Amide1	0.50	12	0.315
C	Carbonyl	3.60	30.7	0.689
O	Carbonyl	3.05	79	–0.601
N	Amide2 (attached to sp2 carbon)	3.40	141	–0.476
H	Amide2	0.50	12	0.349

Table A7. Lennard-Jones parameters for MTNI.

Site	Molecule	σ (Å)	ε (K)	q(e)
N	Nitro	2.90	30	0.742
O	Nitro	2.70	42	–0.404
N	Sp2	3.20	57	–0.529
C	Methyl	3.75	98	0.236
N	Ring	3.40	141	–0.047
C	Nitro	3.60	30.7	0.403, –0.199, 0.334

Table A8. Lennard-Jones parameters for TATB.

Site	Molecule	σ (Å)	ε (K)	q(e)
C_α	Nitro	3.60	30.7	0.061
C_α	Amine	3.60	30.7	0.076
N	Nitro	2.90	30	1.131
N	Amine	3.26	160	–1.110
O	Nitro	2.70	42	–0.548
H	Amine	0.50	12	0.519

Table A9. Bond parameters for DNAN.

Bond	Molecule	Equilibrium Bond Length (Å)	Force constant (kcal/mol)
O-N	nitro	1.22	866.45
N-C	nitro, aromatic	1.49	363.08
C-C	aromatic, aromatic	1.4	528.27
C-O	aromatic, ether	1.41	480.35
O-C	ether, methyl	1.41	289.56

Table A10. Bond parameters for MNA.

Bond	Molecule	Equilibrium Bond Length (Å)	Force constant (kcal/mol)
O-N	nitro	1.22	872.54
N-C	nitro, aromatic	1.49	361.61
C-C	aromatic, aromatic	1.4	529.35
C-N	aromatic, amine	1.35	528.94
N-C	amine, methyl	1.44	413.41
N-H	amine	0.99	614.35

Table A11. Bond parameters for DNP.

Bond	Equilibrium Bond Length (Å)	Force constant (kcal/mol)
C-C	1.40	485.9
C=N	1.30	646.2
C-Nitro	1.43	409.6
N-C	1.34	566.2
N-H	0.99	601.8
N-O	1.18	956.5
C=C	1.35	636.4
N-N	1.30	557.8

Table A12. Bond parameters for NTO.

Bond	Molecule	Equilibrium Bond Length (Å)	Force constant (kcal/mol)
H-N	Amide	0.99	611.64
N-C	Amide, Carbonyl	1.37	428.83
N-N	Amide, Sp2	1.35	435.90
N=C	Sp2	1.25	932.04
C-N	Sp2, Amide	1.35	459.76
C=O	Carbonyl	1.19	1061.00
C-N	Sp2, Nitro	1.44	377.16
N-O	Nitro	1.18	1041.04

Table A13. Bond parameters for MTNI.

Bond	Molecule	Equilibrium Bond Length (Å)	Force constant (kcal/mol)
N-O	nitro	1.17	1007
N-C	nitro	1.44	388.30
C=C	ring	1.35	621.20
C=N	ring	1.27	723.70
C-N	ring	1.34	535.40
N-C	sp2 nitrogen	1.34	535.4
N-C	sp2 carbon	1.33	529.4

Table A14. Bond parameters for TATB.

Bond	Molecule	Equilibrium Bond Length (Å)	Force constant (kcal/mol)
O-N	nitro	1.22	872.66
N-H	amine	1.01	614.44
N-C	nitro	1.49	361.66
N-C	amine	1.44	529.23
C-C	aromatic	1.40	529.43

Table A15. Bending parameters for DNAN.

Angle	Molecule	Equilibrium Bond Angle (degree)	Force constant (kcal/mol)
C-O-C	ether, aromatic	122	97.94
O-N-O	Nitro	125	181.13
O-N-C	nitro, aromatic	117.5	167.89
C-C-C	aromatic, aromatic, aromatic	120	189.7
O-C-C	ether, aromatic, aromatic	125	138.72
N-C-C	nitro, aromatic, aromatic	120	154.79

Table A16. Bending parameters for MNA.

Angle	Molecule	Equilibrium Bond Angle (degree)	Force constant (kcal/mol)
H-N-C	amine	117.77	72.9
O-N-O	nitro	125	181.1
O-N-C	nitro, aromatic	117.5	167.9
C-C-C	aromatic, aromatic, aromatic	120	189.4
N-C-C	amine, aromatic, aromatic	120	145.4
N-C-C	nitro, aromatic, aromatic	120	154.8

Table A17. Bending parameters for DNP.

Bond	Equilibrium Bond Angle (degree)	Force constant (kcal/mol)
H-N-C	127.24	75.22
N-C=C	108.77	296
N=C-Nitro	120.82	130.6
O-N-O	126.7	182.2
N-N-C	101.5	317
C=C-C	101.21	317
C-C=N	113.43	290.5
C=C-Nitro	130.73	107.8
C-C-Nitro	125.73	123.2
C=N-N	111.97	322.8
C-N-O	117.16	144.8
H-N-N	121.14	80.65
N-C-Nitro	120.49	122

Table A18. Bending parameters for NTO.

Bond	Molecule	Equilibrium Bond Angle (degree)	Force constant (kcal/mol)
C-N-C	sp2, amide1, carbonyl	106.88	2514.45
H-N-C	amide2, carbonyl	125.93	83.645
H-N-N	amide2, sp2	120.44	87.99
H-N-C	amide1, carbonyl	125.94	80.57
H-N-C	amide1, sp2	127.18	73.36
N-C-N	Nitro,sp2, amide1	121.55	149.87
N-N-C	amide2, sp2,	103.74	2401.53
N-C-N	sp2, sp2, Nitro	124.47	149.89
N-C-N	amide1, carbonyl,amide2	101.77	1347.10
N-C-O	amide1, carbonyl	129.18	136.36
O-C-N	carbonyl, amide2	129.05	231.29
O-N-O	Nitro	127.18	182.20
O-N-C	Nitro, sp2	118.10	231.29

Table A19. Bending parameters for MTNI.

Bond	Molecule	Equilibrium Bond Angle (degree)	Force constant (kcal/mol)
O-N-O	Nitro	126.70	182.20
O-N-C	Nitro	117.12, 116.47, 118.01	148.50, 116.50, 140.20
N-C=C	Nitro,Csp2	131.50	110.80
N-C-N	Ring, Nitro	123.13	160.40
C=C-N	Ring, Amide	107.37	296.70
C-N-C	Ring	103.50	337.70
C-N-C	Ring, Methyl	130.6	130.60
N-C=N	Ring, sp2	114.46	283.70

Table A20. Bending parameters for TATB.

Angle	Molecule	Equilibrium Bond Angle (degree)	Force constant (kcal/mol)
H-N-C	amine	119.80	73.86
O-N-O	nitro	125.00	181.13
O-N-C	nitro, aromatic	117.5	167.91
C-C-C	aromatic, aromatic, aromatic	120	189.41
N-C-C	amine, aromatic, aromatic	120	145.43
N-C-C	nitro, aromatic, aromatic	120	154.81

Table A21. Torsional parameters for DNAN.

Dihedral	Molecule	n	Phase angle (degree)	C_i [kcal/mol]
C-C-C-C	aromatic	2	180	15.230
O-N-C-C (ortho)	nitro, aromatic	1, 2, 3, 4	0, 0, 0, 0	0.065, –0.202, 0.085, 0.571
O-N-C-C (para)	nitro, aromatic	1, 2	180, 180	–0.136, 4.351
C-O-C-C	ether, aromatic	1, 2	180, 180	0.663, 1.467

Table A22. Torsional parameters for MNA.

Dihedral	Molecule	n	Phase angle (degree)	C_i [kcal/mol]
C-C-C-C	Aromatic	2	180	15.230
O-N-C-C (ortho)	nitro, aromatic	1, 2	180, 180	–0.136, 4.351
C-N-C-C	amine, aromatic	2, 4	180, 180	–0.308, 3.003

Table A23. Torsional parameters for DNP.

Dihedral	Molecule	n	Phase angle (degree)	C_i [kcal/mol]
C=C-N-N, C-N-N=C	Ring	1	180	111.600
N-N=C-C, N=C-C=C	Ring	1	0	134.400
C-C=C-N	Ring	1	180	144.00
O-N-C-C	Nitro	1,2	180	–0.082, 3.29

Table A24. Torsional parameters for NTO.

Dihedral	Molecule	N	Phase angle (degree)	C_i [kcal/mol]
C-C=N-N	ring	1	180	50.62
C=N-N-C, N-C-N-C, C-N-C=N	ring	1	180	69.83
N-N-C-N	ring	1	180	104.60
O-N-C-C	nitro	1,2	180, 180	–0.082, 3.29

Table A25. Torsional parameters for MTNI.

Dihedral	Molecule	n	Phase angle (degree)	C_i [kcal/mol]
N=C-N-C	Ring	1	180	123.40
C-N-C=C	Ring	1	180	143.80
N-C=C-N	Ring	1	180	125.30
C=C-N=C	Ring	1	180	134.80
C-N=C-N	Ring	1	180	126.20
O-N-C-N	Nitro	1, 2	180, 180	–0.059, 1.218
O-N-C=C	Nitro	1, 2	0, 0	0.065, 0.584

Table A26. Torsional parameters for TATB.

Dihedral	Molecule	n	Phase angle (degree)	C_i [kcal/mol]
C-C-C-C	ring	2	180	15.230
O-N-C-C	nitro	1, 2, 3, 4	180, 180, 180, 180	0.023, 4.755, 0.017, -1.014
H-N-C-C	amine	1, 2, 3, 4	0, 180, 0, 180	0.023, 3.015, –0.451, 0.119

REPORT DOCUMENTATION PAGE

Form Approved
OMB No. 0704-0188

1. REPORT DATE (DD-MM-YYYY)	2. REPORT TYPE	3. DATES COVERED (From - To)
15-11-2010	Final	

4. TITLE AND SUBTITLE
Prediction of Environmental Impact of High-Energy Materials with Atomistic Computer Simulations

5a. CONTRACT NUMBER
W9132T-06-2-0027

5b. GRANT NUMBER

5c. PROGRAM ELEMENT

6. AUTHOR(S)
Nandhini Sokkalingam , Jeffrey J. Potoff , Veera M. Boddu , Stephen W. Maloney , and Joyce C. Baird

5d. PROJECT NUMBER

5e. TASK NUMBER

5f. WORK UNIT NUMBER

7. PERFORMING ORGANIZATION NAME(S) AND ADDRESS(ES)
US Army Engineer Research and Development Center (ERDC)
Construction Engineering Research Laboratory (CERL)
PO Box 9005,
Champaign, IL 61826-9005

8. PERFORMING ORGANIZATION REPORT NUMBER
ERDC/CERL TR-10-26

9. SPONSORING / MONITORING AGENCY NAME(S) AND ADDRESS(ES)
US Army Armament Research, Development and Engineering Center (ARDEC)
Energetics and Warheads Division
Picatinny Aresenal, NJ 07806-5000

10. SPONSOR/MONITOR'S ACRONYM(S)
ARDEC

11. SPONSOR/MONITOR'S REPORT NUMBER(S)

12. DISTRIBUTION / AVAILABILITY STATEMENT
Approved for public release; distribution is unlimited.

13. SUPPLEMENTARY NOTES

14. ABSTRACT

This work used atomistic MD simulations to predict environmental impact of six energetic materials, 2,4-dinitroanisole (DNAN), N-methyl-p-nitroaniline (MNA), 3,5-dinitropyrazole (DNP), 3-nitro-1,2,4-triazol-5-one (NTO), 1-methyl-2,4,5-trinitroimidazole (MTNI) and 1,3,5-triamino-2,4,6-trinitrobenzene (TATB). Molecular models developed for these compounds were used to determine octanol-water partition coefficient (log Kow) and Henry's law constant (log H). Log Kow was predicted for DNAN and MNA to within ±0.1 log units of experiment, while log H was predicted to within ±1.0 log units. For the remaining four compounds, no experimental data exist for comparison. Predicted log Kow and log H values suggest that these compounds have the potential to cause groundwater contamination. Depending on the values of the partition coefficients, appropriate treatment methodologies can be chosen for each contaminant of interest. In addition to partition coefficients, a variety of thermophysical properties were predicted, including vapor-liquid coexistence curves, critical points, vapor pressure, heats of vaporization, crystal lattice parameters, and solid density. The crystal density and lattice parameters predicted for all energetic materials were in close agreement with experimental data. Overall, these results suggest that empirical force fields, combined with molecular dynamics simulations, provide an accurate methodology for predicting relevant descriptors of environmental fate for energetic materials.

15. SUBJECT TERMS
environmental impact, energetic materials (EM), simulation, munitions waste, hazardous waste

16. SECURITY CLASSIFICATION OF:			17. LIMITATION OF ABSTRACT	18. NUMBER OF PAGES	19a. NAME OF RESPONSIBLE PERSON
a. REPORT	b. ABSTRACT	c. THIS PAGE			19b. TELEPHONE NUMBER (include area code)
Unclassified	Unclassified	Unclassified	SAR	58	